Bolometer Diagnostics on Alcator C-Mod

by

Brian Joaquin Youngblood

Submitted to the Department of Nuclear Engineering
in partial fulfillment of the requirements for the degree of

Master of Science in Nuclear Engineering

at the

MASSACHUSETTS INSTITUTE OF TECHNOLOGY

September 2004

Author .....
Department of Nuclear Engineering
August 27, 2004

Certified by .....
Ian H. Hutchinson
Professor of Nuclear Engineering
Thesis Supervisor

Certified by .....
Ronald R. Parker
Professor, Departments of Nuclear and Electrical Engineering
Thesis Reader

Accepted by .....
Jeffrey A. Coderre
Chairman, Department Committee on Graduate Students

Bolometer Diagnostics on Alcator C-Mod

by

Brian Joaquin Youngblood

Submitted to the Department of Nuclear Engineering
on August 27, 2004, in partial fulfillment of the
requirements for the degree of
Master of Science in Nuclear Engineering

Abstract

Bolometry is a diagnostic technique common to most tokamak fusion experiments. Bolometers are so widespread because they provide an important measure of the energy lost from confined plasmas as radiation, as well as being relatively simple and resilient in their construction. Here the bolometric diagnostics of the Alcator C-mod tokamak, their function, limitations, and the details of their calibration, operation, and maintainance are covered. In addition, the results of a variety of investigations into the behavior of C-mod plasmas as observed by bolometers are presented and discussed. The measurements dealt with are either measurements of total power radiated by the plasma or measurements of radial emissivity profiles. Measurements of the first kind are suitable for studying the effects of factors like net input power while measurements of the second kind are useful for studying the effects of factors like local temperature profiles and plasma composition.

Thesis Supervisor: Ian H. Hutchinson
Title: Professor of Nuclear Engineering

Thesis Reader: Ronald R. Parker
Title: Professor, Departments of Nuclear and Electrical Engineering

Acknowledgments

There are many people without whom this thesis would not be possible and many without whom the experience of producing it would not have been the same. I want to thank them all, but since space and memory are limited I will have to restrict myself to thanking only a few (mostly from the lab) and hope that the rest will forgive me. First, I thank my parents for a lifetime of support and encouragement. I also thank my advisor, Ian Hutchinson, for his invaluable assistance and tremendous patience. I also offer my gratitude to my other professors, Ron Parker, Kim Molvig, Jeffrey Freidberg, Miklos Porkolab, and Bruno Coppi who have taught me a great deal. Special Thanks go to the administrative staff of the Nuclear Engineering Department and PSFC, Valerie Censabella, Clare Egan, Heather Geddry, Dorian McNamara, Megan Tabak, and Carol Arlington for all of their help and kind efficiency. Many thanks are due to the scientists and staff of the Alcator project as well. In my case particular thanks are due to Bruce Lipschultz, Earl Marmar, Brian LaBombard, Catherine Fiore, Steve Wolfe, Bob Granetz, Tom Toland, Dave Bellofato, Josh Stillerman, Sam Pierson, and Henry Savelli. Finally, I must thank my fellow students and friends especially Bo Bai, Tom Jennings, Vincent Tang, Tim Graves, Kirill Zhurovich, John Liptac, Tae Kyun Chung, Howard Yuh, Jerry Hughes, Davis Lee, Justin Sarlese, Sanjay Gupta, Chris Boswell, Eric Edlund, and my officemates: Noah Smick, Balint Veto, Brock Bose, and Liang Lin for their help in making the whole thing a lot of fun.

Contents

List of Figures

Chapter 1

Introduction

Thermonuclear fusion is a promising method of advanced alternative energy production. Fusion uses fuels that are ample and widespread rather than scarce fossil fuels. A fusion reactor would produce no dangerous or environmentally harmful pollutants. Finally, once decomissioned the activated vacuum vessel of a fusion device would remain radioactive for far less time than the radioactive wastes typically produced by fission reactors. For these reasons fusion represents a clean, long-lasting, and (hopefully) cheap source of energy. The possibility such an energy source is so attractive that research into the construction of a working fusion reactor has therefore been pursued for fifty years.

The obstacle that has stood in the way of the goal of fusion energy production is the need to confine the particles and energy of a hot plasma in a small volume for an amount of time sufficient to allow enough fusion reactions to occur. This problem is still unresolved and makes the study of the means by which confinement is lost critically important.

One of the principal ways energy is lost from the plasma is by means of electromagnetic radiation. Various processes occurring in the plasma give rise to radiation. Chief among these are bremsstrahlung, cyclotron, and line radiation. This thesis is a study of the bolometer system on the Alcator C-Mod tokamak [1] which measures the spatial profile of the radiation emitted by the plasma.

1.1 Fusion Research

The bolometer diagnostic detailed in this thesis is used to study the plasma in an experimental tokamak built as a step toward an energy producing fusion reactor. For this reason it is important to present some background information about both magnetic confinement fusion research in general and the Alcator C-Mod tokamak in particular. This section will provide an outline of the history of fusion research, a brief introduction to the magnetic confinement of plasmas, and some details about the C-Mod tokamak.

1.1.1 History

American, British, and Soviet fusion research was declassified in 1958. Ten years after the general declassification of fusion research it was demonstrated that with the technology then available the confinement achieved in tokamak devices was far superior to that possible with magnetic mirrors and stellarators. Since then fusion research has been focused on the tokamak magnetic confinement concept and that concept remains, of the various magnetic and other confinement schemes, the one in the most advanced stage of development.

Recently, there has been a resurgence in the research of stellarator technology. This rekindling of interest in the stellarator approach to magnetic confinement has resulted in the construction of new stellarator devices. These new devices, built using modern design technology and manufacturing techniques, are now approaching the theoretical capabilities of the stellarator design. Other magnetic confinement approaches, including reversed field pinches, dipoles, and several variations on the tokamak and stellarator designs are also investigated, though not in as many places. Two final things to note: first, plasma confinement has many more applications than fusion research and there are a great many confinement schemes ranging from purely electrostatic Penning traps used to study non-neutral plasmas to cusp fields used to investigate solar and space physics; second, research on fusion via laser-driven inertial "confinement" has not been mentioned, though this field has experienced significant

development of late.

1.1.2 Fusion and Tokamaks

Fusion

The success of any plasma confinement method or device built to pursue the possibility of fusion energy production is generally gauged on the basis of how close one can come to maintaining sustained fusion reactions in the device. The condition that must be met for fusion to be sustained is easy to express (though not so easy to satisfy!): The rate at which energy is added to the plasma system must (including energy from fusion reactions) equal the rate at which energy is lost by the plasma. This is expressed as the power balance equation

$$P_{\alpha fus} + P_{heating} = P_{loss} \tag{1.1}$$

Currently, the best candidate reaction for an energy producing fusion device is the D-T reaction

$$^2H +^3 H \rightarrow n +^4 He + 17.6MeV \tag{1.2}$$

Simple kinematics tells us that the neutron carries 4/5 of the energy released in the reaction or 14.1 MeV while the alpha particle carries only 3.5 MeV. This is important for power balance because only power added by the charged alpha particles is present in the $P_{\alpha fus}$ since the neutrons are not confined and are instantly lost from the plasma. The confined plasma therefore gains $Q_\alpha = 3.5MeV$ of energy for each fusion reaction. The rate of these energy contributing reactions is determined by the D-T fusion reaction cross-section. We will use the value of this cross-section that yields the minimum possible ignition condition (this occurs at a plasma temperature of 27keV).

$$< \sigma v >= 6 \times 10^{-22} m^3 s^{-1} \tag{1.3}$$

Now we can fill in the factors in an expression for the first term of the power balance

equation for a 50-50 mixture of deuterium and tritium ($n_D = n_T = n/2$) and equal temperatures for all species.

$$P_{\alpha fus} = \frac{1}{4} n_e^2 < \sigma v > Q_\alpha \tag{1.4}$$

where n_e is the electron density. The rate at which energy is lost from the plasma by diffusion is proportional to the energy contained in the plasma. The energy contributed by each species in the plasma is given by the equation for the energy in a monatomic ideal gas of the same temperature $E = 1.5nT$. If we ignore radiation losses (something that will later be shown to be a mistake) and recognize that the plasma is quasineutral then the last term in the power balance can be written

$$P_{loss} = \frac{3 n_e T_e}{\tau_E} \tag{1.5}$$

The τ_E in the constant of proportionality is the energy confinement time.

If the fusion power matches the power lost then the plasma is said to be ignited. Our expressions for the corresponding terms in the power balance equation allow us to obtain a condition for plasma ignition in terms of electron density and energy confinement time as follows

$$\begin{aligned} 3 n_e T_e \frac{1}{\tau_E} &= \frac{1}{4} n_e^2 < \sigma v > Q_\alpha \\ 12 T_e &= n_e \tau_E < \sigma v > Q_\alpha \\ \frac{12 T_e}{< \sigma v > Q_\alpha} &= n_e \tau_E \\ 1 \times 10^{20} m^{-3} s &\approx n_e \tau_E \end{aligned}$$

To obtain the final equation we used the same T_e (27keV) used to obtain (1.3)[2].

Tokamaks

Charged particles, like those that make up a plasma, are constrained to move in a helical path around magnetic field lines with a frequency $\omega_c = qB/m$ and a gyro-

radius $\rho = \frac{1}{\omega_c}\sqrt{2E/m}$. This is the basis for the magnetic confinement of plasmas. The tokamak confinement concept, at its most basic level, consists of enclosing the plasma in a toroidal vacuum vessel and applying a closed toroidal magnetic field using external coils. Additional fields are required to stabilize the system and prevent it from expanding radially, notably a poloidal field, conveniently produced by the current in the plasma itself, is necessary. The combination of the toroidal and poloidal magnetic fields results in the tokamak having helical field lines.The plasma is confined in the toroidal direction because the flux surfaces are closed in that direction. Several limits on the parameters of the system are imposed by its physics and these limits constrain what one can do with a tokamak and how one can do it [2, 3].

Beta Limits

The parameter β is the ratio of the plasma kinetic pressure to the magnetic field pressure. Generally, one wants to design a tokamak so that β is as high as possible so that a higher plasma pressure may be confined per unit of field strength, but there are strong equilibrium and stability limits imposed on β values. There are many possible forms for β. Two of the most useful of these are

$$\beta_p = \frac{2\mu_0 < p >}{B_\theta^2(a)} \tag{1.6}$$

and

$$\beta_t = \frac{2\mu_0 < p >}{B_\phi^2(0)}. \tag{1.7}$$

where B_θ and B_ϕ are the poloidal and toroidal magnetic field magnitudes, respectively. The poloidal beta value (β_p) is the ratio of average plasma kinetic pressure ($< p >$) to the pressure of the poloidal magnetic field at the edge of the plasma. In order to have a (circular) plasma in equilibrium the poloidal beta must satisfy

$$\beta_p \leq \frac{1}{\epsilon} \tag{1.8}$$

where ϵ is the inverse aspect ratio of the toroidal plasma $\epsilon = a/R$. The physical reason

for this limit on β_p is that if the ratio between the kinetic and magnetic pressures is larger than the limiting value, the last closed flux surface of the confining field will infiltrate the main body of the plasma causing the plasma to flow out and confinement to be lost.

The toroidal beta value is defined in a manner similar to the poloidal beta. The difference is that the edge poloidal magnetic field strength is replaced by the on axis toroidal field strength. To be stable to kink modes the plasma must satisfy the Troyon limit

$$\beta_t \leq 0.03 \times \frac{Ip[MA]}{aB_\phi(0)}. \tag{1.9}$$

If the plasma is stable to kinks it should also be stable to ballooning modes which impose a slightly higher limit on β_t. The limiting value scales linearly with the elongation κ (vertical size/minor radial size) of the plasma so tokamaks are usually built to have plasmas with $\kappa > 1$.

1.1.3 Alcator C-Mod

Figure 1-1 shows a cross-section of the Alcator C-mod tokamak. C-mod has a compact, high field torus design. C-mod typically operates at a toroidal field strength of 5-6 T and a plasma current of a little over 1MA though it is designed to be capable of operation with a 9 T field and 3MA current [1]. The average electron density of most shots is between 1 and 4 $\times 10^{20} m^{-3}$. The tokamak has a major radius of 0.67 m and a minor radius of 0.21 m (see Figure 1-1).

1.2 Plasma Radiation

This section gives some details about the most significant plasma radiation processes.

Cyclotron Radiation

Charged particles undergoing acceleration emit electromagnetic radiation. Since magnetically confined particles orbit about field lines they are continuously accelerated

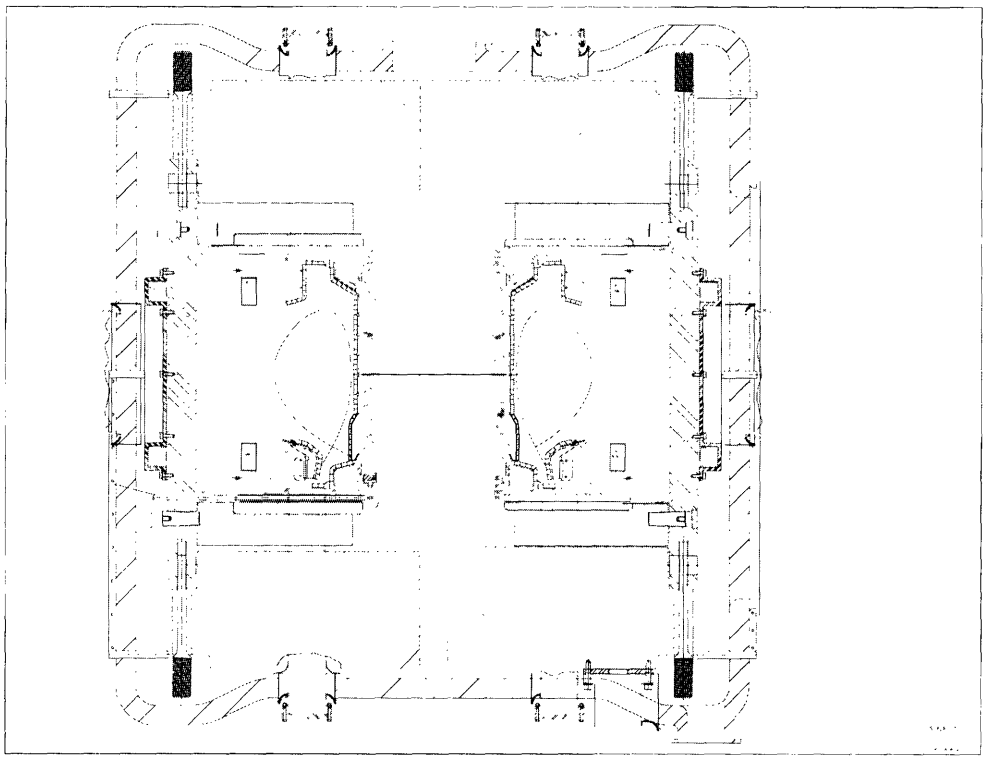

Figure 1-1: A cross-section of the C-mod Tokamak.

and so are constantly emitting. The acceleration of a particle in a circular cyclotron orbit is

$$a_{cyc} = \omega_c^2 \rho \tag{1.10}$$

where ω_c is the cyclotron frequency qB/m and ρ is the particle gyroradius $v_\perp/\omega_c$. The rate of energy emission from a nonrelativistic particle with acceleration a is given by

$$\frac{dW}{dt} = \left(\frac{q^2}{6\pi\epsilon_0 c^3}\right) a^2 \tag{1.11}$$

If we take the velocity of the confined particles perpendicular to the magnetic field confining them to be $v_\perp = \sqrt{2T/m}$ then by (1.10) and (1.11) and the definition of ω_c, the rate of energy emisson due to a single particle is

$$\begin{aligned} \frac{dW}{dt} &= \left(\frac{q^2}{6\pi\epsilon_0 c^3}\right)\left(\frac{qB}{m}\right)^4\left(\frac{2T}{m}\right)\left(\frac{m}{qB}\right)^2 \\ &= \left(\frac{q^4 B^2}{3\pi\epsilon_0 (mc)^3}\right) T \end{aligned}$$

The power density of cyclotron emissions due to a single species is obtained by multiplying the last expression by the particle density of that species and using its charge, mass, and temperature. Since electrons are much less massive than any of the other plasma particles their contribution to plasma cyclotron emission is by far the greatest even when impurities present in the plasma are taken into account.

To this point the discussion of cyclotron emissions from the plasma was much simplified, particularly in that it deals only with emissions at the fundamental cyclotron frequency. Radiation is also emitted at the harmonics of the cyclotron frequency but at considerably lower levels. Also missing from the treatment is a consideration of how much energy emitted by the plasma particles is actually lost. The plasma is opaque to the fundamental electron cyclotron frequency and the lowest harmonics so the rate of energy loss from the plasma due to cyclotron emissions is small, especially compared to losses due to other radiating processes. In the operating regime of current tokamaks cyclotron losses are negligible, though they are useful for temperature

measurements.

Bremsstrahlung

In addition to undergoing acceleration due to their orbits in a confining field the particles in a plasma are accelerated by collisions with other particles. This is called bremsstrahlung or braking radiation and it constitutes the most significant radiation power loss process in a pure hydrogen isotope plasma.

The maximum acceleration due to a Coulomb collision between an electron and an ion of charge Z is given by

$$a_{coll} = \frac{Ze^2}{4\pi\epsilon_0 m_e b^2} \tag{1.12}$$

where b is the impact parameter. We can make the approximation that the collision lasts for a time $2b/v$ with $v = \sqrt{3T/m}$. Putting (1.12) into (1.11) and multiplying by the duration of the collision gives the energy emitted in each collison in terms of its impact parameter and plasma parameters. Integrating over impact parameters (bearing in mind that the minimum possible impact parameter is the electron de Broglie wavelength) gives an approximation close to the actual bremsstrahlung power value which is most accurately given by

$$\frac{P_{brems}}{n_e n_i} = \frac{e^6 Z^2 T_e^{1/2}}{6\sqrt{3/2}\pi^{3/2}\epsilon_0^3 c^3 m_e^{3/2} h} \tag{1.13}$$

as the equation for the power density of bremsstrahlung emissions due to collisions between electrons and Z ions.

The classical treatment above must be corrected for quantum mechanical effects by multiplying P_{brems} by the Gaunt factor g. In a fusion plasma g is near unity.

Line Radiation

In a pure hydrogen isotope plasma bremsstrahlung radiation represents the minimum possible energy loss not due to transport. In a real plasma with impurities, line

radiation from those impurities is usually comparable to or greater than that due to electron bremsstrahlung.

The radiated power density due to impurity species Z has the form [4]

$$P_{rad,Z} = n_Z n_e f_Z(T_e). \tag{1.14}$$

The temperature dependence $f_Z(T_e)$, usually obtained from theoretical calculations, is complicated and different for every species. Nevertheless, some accurate general statements can be made about the temperature behavior of P_{rad}. Above 1keV temperatures low-Z impurities do not contribute to plasma line radiation because they no longer have electrons to produce line emissions. In a tokamak, line radiation from low-Z impurities comes from the edge where the temperature is sufficiently low. High-Z impurities are another story, they retain some electrons through all or most of the plasma and so radiate everywhere. In addition to radiating over a broader range of temperatures high-Z impurities have an $f_Z(T_e)$ that is on average an order of magnitude greater than low-Z impurities.

1.3 The Significance of Radiation Measurements

Radiation emitted by plasma particles and not reabsorbed by the plasma represents a loss of energy from the plasma system. The energy lost in this way is a significant part of the loss term in the power balance equation (1.1). For this reason it is important to observe as closely as possible the radiation emitted by the plasma.

Several diagnostics used to study fusion plasmas depend on measuring the radiations of that plasma. The temperature can be measured by means of the electron cyclotron emissions of the plasma. The value of Z_{eff} can be determined by measuring the bremsstrahlung radiation while excluding line radiation. Spectral measurements are used to obtain the (relative) quantities of different substances in the plasma. One of the bolometer diagnostics covered by this thesis is used to determine the total power radiated from a plasma in the ultra-violet and x-ray regions of the EM spec-

trum. The other is an array of identical bolometers used to construct radial profiles of the plasma volume emissivity [5]. In a tokamak radiation in this range is dominated by line emissions.

Chapter 2

Bolometer Operation

The Alcator C-Mod tokamak is equipped with two types of bolometric detector. One type is based on the thermal response of a metal foil to impinging photons and the other is based on the photodiode behavior of a semiconductor. At present there are two diagnostics of each type used to study plasma radiation in the tokamak. For each type there is a diagnostic used to estimate plasma radiated power and another used to obtain radial profiles of the plasma emissivity.

2.1 Detectors

2.1.1 Foil Detectors

The first type of bolometeric detector to discuss is the foil bolometer. As mentioned above these detectors work because incoming radiation heats a small piece of metal foil (in the case of the Alcator diagnostics, gold foil)[6]. The heating of the foil is produced primarily by photoelectric absorbtion. The foil is in thermal contact over its whole surface with a thin meander resistor see (Fig.2-1) for a schematic of the meander resistor. Temperature changes in the foil are accompanied by a decrease in the resistivity of the gold resistor. A bridge circuit, shown schematically below (Fig. 2-2), is used to convert this resistivity change to a voltage signal which is amplified and recorded.

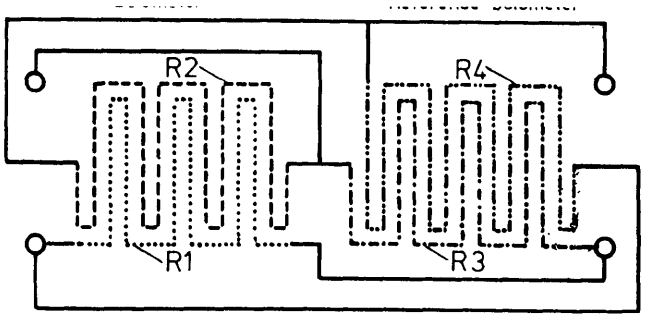

Figure 2-1: Schematic diagram of two of the detector resistors.

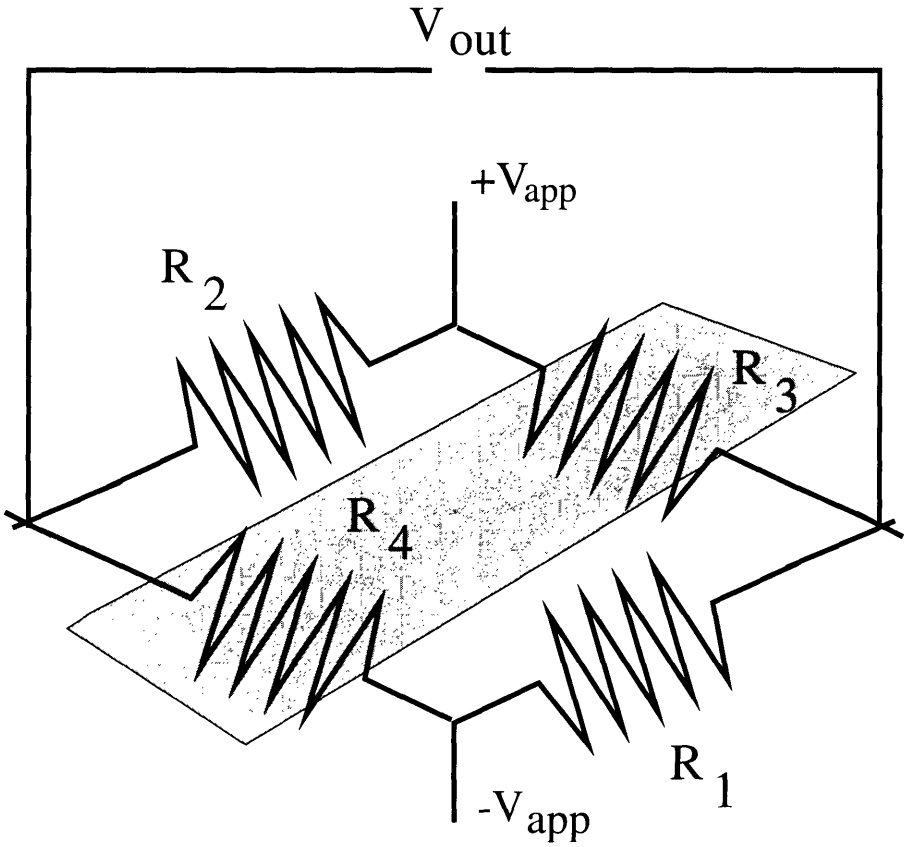

Figure 2-2: Two of the foils are exposed and two are covered.

When no radiation is inicident on the bolometers, all resistances are equal to a common value, R. The signal from the bridge circuit is then

$$V_{out} = \frac{V_{app}}{R}\frac{\Delta R}{2} \tag{2.1}$$

where V_{out} is the voltage measured across the circuit as shown in Figure 2-2, V_{app} is the total voltage applied to power the bridge, and ΔR is the change in the resistance of the exposed resistors. If we can assume that the resistance R varies linearly with with temperature T, a valid assumption for gold near room temperature, then we can write

$$R = \alpha \Delta T + R_{rt} \tag{2.2}$$

with R_{rt} as the room temperature resistance of a single resistor element and α as the slope of the temperature-resistance relation (with units $\frac{\Omega}{K}$ for example) V_{out} is then related to the change in foil temperature by

$$\Delta T = \frac{R_{rt}}{|\frac{\alpha}{2}|\left(\frac{V_{app}}{V_{out}} - 2\right)} \approx \frac{R_{rt}}{\alpha/2}\frac{V_{out}}{V_{app}} \tag{2.3}$$

The power absorbed by the detector (as a function of time) is related to its temperature by

$$P_{det}(t) = \frac{1}{\kappa}\left(\Delta T(t) + \tau_c \frac{d\Delta T}{dt}\right) \tag{2.4}$$

where τ_c is the cooling time and κ is a calibration constant. The relation between P_{det} and the power radiated by the plasma will be discussed in the next chapter.

The advantages of foil type bolometers are their simplicity and reliability. The bridge circuit arrangement with shielded detectors used as the reference resistors makes the elimination of signals due to background temperature changes automatic. The detectors can be calibrated in place (see below) and do not need to be adjusted once installed. Detector sensitivity is only slightly susceptible to neutron bombardment. Additionally foil detectors have no spectral resolution. The gold foil bolometers used on C-mod measure all radiation in their range of sensitivity. One important con-

sequence of this feature is that identifying the source of the measured radiation is not possible with any certainty using just bolometer information.

There are two main disadvantages to using foil type bolometer detectors. The first is that the foil is heated by neutral particles as well as by EM radiation. There is therefore no way to distinguish between these two channels of plasma energy loss using foil bolometers alone. The second drawback is that foil bolometers are slow. The value of τ_c, the cooling time has a lower limit which in turn limits the time resolution of the diagnostic.

2.1.2 AXUV(Diode) Detectors

A photodiode allows more or less current to pass depending on how much light is incident on it. The photodiodes used as bolometric detectors on C-Mod are sensitive to light in the soft x-ray to ultraviolet range responding best from 20eV to 10keV [7].

Advantages of the diode detectors over the foil detectors are their faster time response, their insusceptibility to heating by neutrals, and a simpler circuit to tune. The major problem with using these detectors is that their spectral response is less certain than for foil bolometers and the absolute calibration is known to vary depending on environment. This type of detector is especially susceptible to acquiring thin coatings of material in the course of tokamak conditioning which play havoc with the calibrations.

2.2 Arrangement

2.2.1 Detector Arrays

Both of the bolometer arrays (foil and diode) used to obtain plasma emissivity profiles are contained in a box mounted at K-Port on C-Mod (see Fig. 2-3). The box is at about the midplane and the apertures face A-port. Each array consists of sixteen viewing chords which span the minor radius of the tokamak.

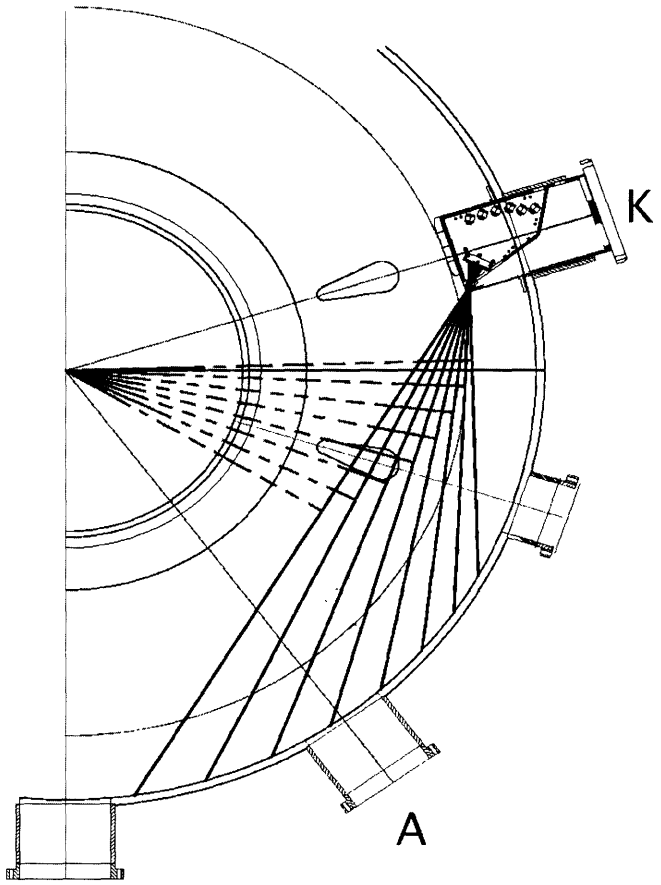

Figure 2-3: Bolometer Box Arrangement. Solid lines: Sample viewing chords; Broken lines: Tangency radii.

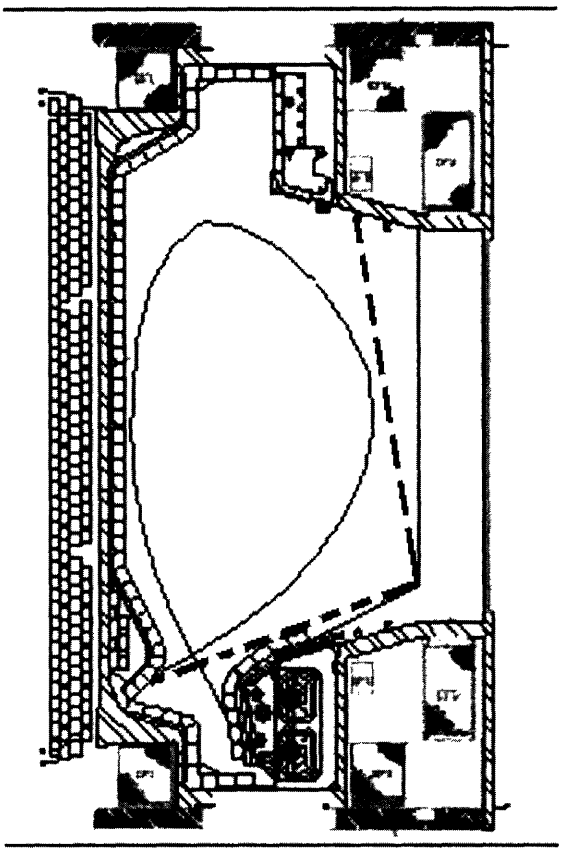

Figure 2-4: 2π Bolometer View; Solid lines: Theoretical; Broken lines: With limiters and tiles in place.

2.2.2 2π Detectors

The 2π foil and diode detectors are both located outside the plasma and considerably below the midplane. Figure 2-4 shows that these detectors admit light from an entire cross-section of the confined plasma, but exclude the divertor region.

2.3 Calibration of Foil Bolometers

2.3.1 Electronics

All the detector amplifiers have to be periodically adjusted to minimize voltage baseline offsets, though small offsets are removed when the data is analyzed. The foil bolometer channels must have a 5kHz AC signal applied across their bridge circuits.

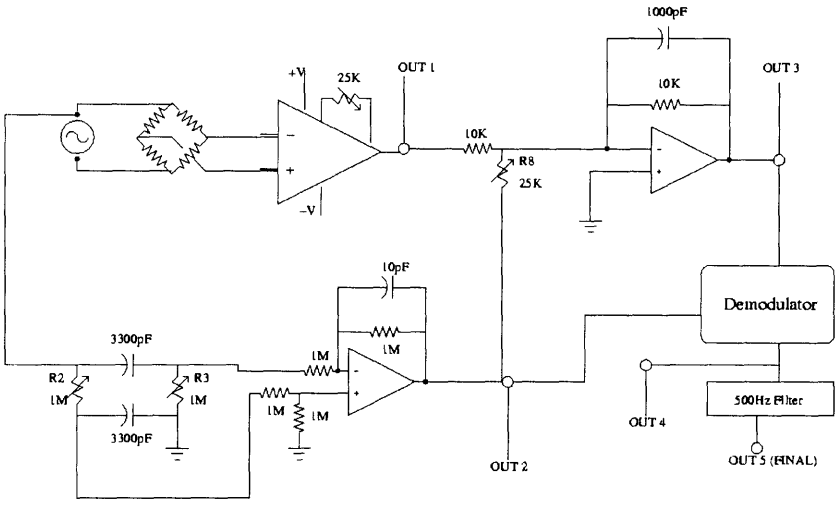

Figure 2-5: Simplified circuit diagram

Figure 2-5 is a simplified circuit diagram for a single foil bolometer channel. The main parts of the circuit are the detector itself, the instrument amplifier, a phase shifter, a nulling circuit, and a (synchronous) demodulator. When calibrating/tuning the bolometer electronics typically only the variable resistors labeled R2, R3, and R8 on the circuit diagram are adjusted. Note that all of the IC components are powered at 12V.

Amplifier

The instrument amp is mostly for adjusting the offset of the detector signal. However the $10k\Omega$ range variable resistor has to be changed only occaisionally. The offset signal coming from the detector channel (OUT 1 in the figure) is fed into an oscilloscope for use in later calibration steps.

Phase Shifter

To properly demodulate the detector signal we need a signal that is 180 degrees out of phase with the 5kHz driving signal. The phase shifter portion of our circuit provides this signal but it must be tuned from time to time. To accomplish this the output of the phase shifter (OUT2) is plotted on the other channel of an oscilloscope that is reading OUT1. The variable resistors R2 and R3 are tuned until the desired

half-period phase difference between the two plotted circuit outputs is achieved.

Nulling Circuit

We want to remove as much of the driving signal as possible so we use a nulling circuit (we combine the out-of-phase signals through an op-amp). We want the minimum output (OUT 3) possible from this part of the circuit. The resistor R8 is adjusted to change how much of the phase-shifted signal is added. Since the adjustments to the phase shifter resistors R2 and R3 is done by eye it is usuall necessary to use the output of the nulling circuit to more finely tune the phase shifter to obtain a minimum signal.

Final Steps

The output of the Nulling circuit is synchronously demodulated using the output of the phase shifter as the synchronizing signal. The output of the demodulator is then put through a 500Hz low pass filter (7-pole Bessel) and sent on to the recording electronics. The demodulator (OUT 4) and filter (OUT 5) outputs are checked to make sure nothing goes wrong in those steps.

2.3.2 Time Constant

The time constant for each channel is determined by finding a shot that ends in a disruption and fitting an exponential curve to the end of the raw voltage signal from the detector bridge. An example of such a fit is shown in Figure 2-6 The decay constant of the exponential will be the reciprocal of the channel's cooling time. The cooling time constants of the channels vary between 0.08 and 0.15 seconds.

2.3.3 Sensitivity

The sensitivity of the detector is just a measure of how a measurable quantity, such as the output voltage of the bridge changes in response to a change in incident radiated power [8]. In section (2.1.1) discussing the response of the foil bolometer the

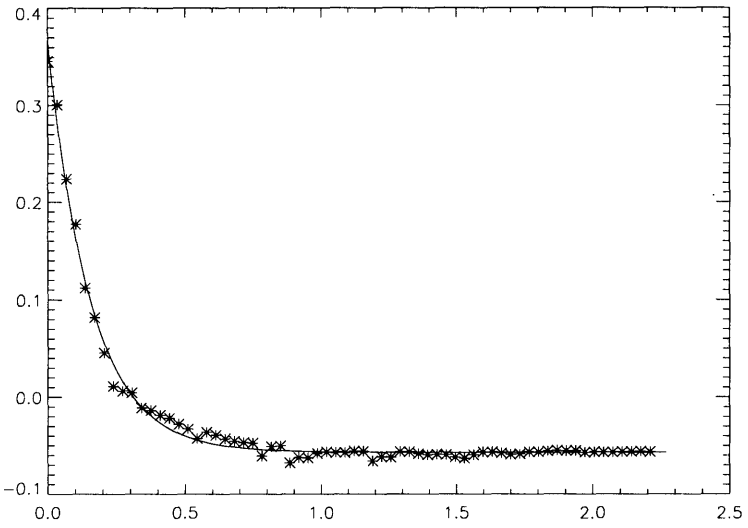

Figure 2-6: Fitting a disruption curve to obtain τ_c

calibration constant κ is a measure of sensitivity. First we consider the sensitivity of the bolometer in a "cold" state. That is, the sensitivity of the bolometer to a single power source absent any other power in the bridge. To do this we simply compare the resistance of the detector when no voltage is applied to its resistance when a known voltage is applied and a known power is dissipated in the foil.

The procedure is to (1) measure the resistance (R) across a detection resistor with the power to the electronics rack turned off, (2) power the electronics and apply a DC voltage of .5V to the bridge, (3) balance the calibration bridge by adjusting the resistance of one leg so that the voltage across the bridge(V_{br})is zero,(4) apply 5V($= V_{app}$) to the bridge and measure the new voltage across the bridge (no longer zero). This procedure is applied to each detector channel. The "cold" sensitivity of the channel defined as

$$S_{cold} = \frac{V_{br}}{V_{app}/2}\frac{1}{P} = \frac{V_{br}}{V_{app}/2}\frac{R}{(V_{app}/2)^2} \tag{2.5}$$

where R is the resistance of one of the detector legs of the bridge, consisting of just one resistor. When the bolometer is in use, the "cold" condition does not hold – in operation each bolometer detector is an AC bridge circuit with a 5Vpp applied voltage, in addition to the radiation falling on the detector, changing the

temperature of the resistors and hence the measured signal. Fortunately, if we know how the detector resistance depends on temperature (or incident power from any source) we can relate the sensitivity at one temperature (such as when the detector is "cold") to the sensitivity at any other temperature.

We can begin with a definition of the sensitivity (S) of the foil bolometer

$$S \equiv \frac{dR}{dP}\frac{1}{R} \tag{2.6}$$

Where R is the resistance of the bolometer element and P is the power incident on the bolometer, either due to radiation or current running through the bridge. If we assume that R varies linearly with P then we can write

$$R = R_0 + \frac{dR}{dP}P \tag{2.7}$$

with $\frac{dR}{dP}$ a constant. The power dissipated in the bolometer is given in terms of the voltage in the resistor by

$$P = \frac{V^2}{R} \tag{2.8}$$

and we can use this expression for the power with the linear equation for resistance to obtain the following quadratic equation for the resistance

$$R^2 - R_0 R - \frac{dR}{dP}V^2 = 0 \tag{2.9}$$

which has as its solution

$$R = \left(R_0 + \sqrt{R_0^2 + 4\frac{dR}{dP}V^2}\right)/2. \tag{2.10}$$

We can see from the definition of S that if we can assume that $\frac{dR}{dP}$ is constant then the ratio between the sensitivities at two different temperatures is the reciprocal of the ratio of the bolometer resistances at those temperatures

$$\frac{S_2}{S_1} = \frac{R_1}{R_2} \tag{2.11}$$

so our solution for R can be used to relate the sensitivity of a bolometer when it is cold to the sensitivity when it has AC current passed through it during operation.

Since we do not necessarily know $\frac{dR}{dP}$ and we do know S_{cold} it is useful to invert (2.6) at $S = S_{cold}$ to get the constant slope. Using this information and taking (2.11) can be rewritten

$$S_{warm} = S_{cold}\frac{2}{\{(1-a) + [(1-a)^2 + b]^2\}} \tag{2.12}$$

where $a = \frac{S_{cold}V_{app}^2}{4R_{cold}}$ and $b = \frac{S_{cold}V_{gen}^2}{R_{cold}}$ and a factor of R_0 was taken out after R_0 was expressed in terms of R_{cold} with V_{app} taken to not be negligible for that purpose.

2.4 Determining the Position of AXUV Tangency Radii

2.4.1 Setup and Procedure

In order to interpret measurements made with bolometers we must, for each detector channel, know the radial position at which the viewing chord corresponding to the detector intersects with a radius of the tokamak at right angles. This is called the radius of tangency of the detector. This radius is not measured directly. The information we have available to determine it is the radial and angular position of the focus of the viewing chords (at the aperture of the AXUV detector) and, for each channel, the radial location of the intersection of the viewing chord with a radius of known toroidal angle. This last value, labeled R_A, is found by placing a small mercury vapor lamp in the tokamak and measuring its distance (in the A-port plane) from the inner wall when the AXUV detector channel of interest has its maximal response. The known distance to the inner wall is added to the measured distance to give R_A The knowns and unknowns of this problem are shown in Figure 2-7 labeled in the following way:

R_b = radial location of the aperture

ϕ_b = angle between the aperture and the center of A-port

R_A = radial location of intersection between the channel viewing chord and the tokamak radius passing through the center of A-port

d_A = the distance along the viewing chord between the aperture and R_A

θ_c = Angle between the radius intersecting the aperture and the channel viewing chord

ϕ_T = Toroidal angle between R_b and the tangency radius

d_T = The distance along the viewing chord between the aperture and the tangency radius

R_T = The radial coordinate of the tangency point that we seek

2.4.2 Calculation

To calculate the tangency radius we need to apply some trigonmetry. We recall the Law of Cosines for a triangle with sides a, b, c opposite angles A, B, C respectively:

$$c^2 = a^2 + b^2 - ab\cos C \tag{2.13}$$

which can be applied to the triangle with sides $a \rightarrow R_b, b \rightarrow R_A, c \rightarrow d_A$(so $C \rightarrow \phi_b$) to obtain the length d_A. Having d_A we can apply (2.13) a second time, but with $a \rightarrow R_b, b \rightarrow d_A, c \rightarrow R_A$(so $C \rightarrow \theta_c$) and rearrange to get

$$\cos\theta_c = \frac{R_b^2 + d_A^2 - R_A^2}{2R_b d_A}$$

Now since the triangle with sides R_T, R_b, d_T is a right triangle we have

$$\begin{aligned} d_T &= R_b\cos\theta_c \\ R_T &= R_b\sin\theta_c \\ \phi_T &= \frac{\pi}{2} - \theta_c \end{aligned}$$

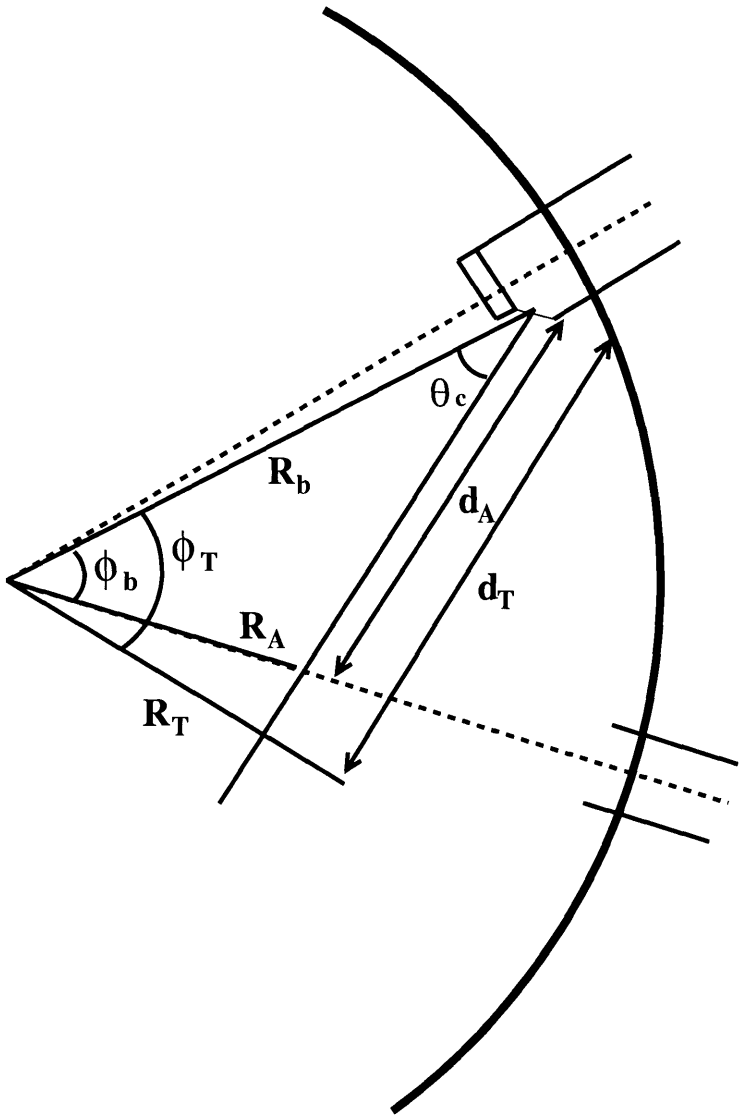

Figure 2-7: Schematic for the determination of tangency radii.

which are the values we wanted.

2.4.3 Results

The critical parameter obtained from these calculations is the value of R_T for each channel. The results are shown in Table 2.1 along with values of R_T obtained from various sources for comparison (all values are in millimeters).

The values in the columns labeled 1999 and 2000 are values reported by Dr. Boivin for measurements made in the '99 and '00 run campaigns(note that my convention for ordering channels is the opposite of his). It is not possible to associate the radii obtained from the design drawing for the AXUV bolometers to particular channels. However, the first and last measurements from the drawing match well with the first and last channels calculated from our most recent measurements. I have listed the drawing measurements in the row of the channel for which they are closest to our R_T values but that correspondence should not be taken too seriously. The channels marked with "*" are broken. These results show that the variation of these measure-

Ch	2002	1999	2000	Drawing
1	921.9	920.6	898.8	920
2	916.2	914.4	893.3	
3	*	906.8	886.5	904
4	900.2	897.6	878.0	
5	892.2	887.6	869.1	880
6	*	875.5	858.1	
7	866.8	861.9	845.6	
8	855.6	846.7	831.6	852
9	834.9	829.8	815.9	
10	821.4	811.3	798.7	820
11	802.1	791.1	779.7	
12	781.4	769.2	759.0	776
13	759.5	745.9	736.9	
14	736.4	721.2	713.4	728
15	712.4	695.1	688.4	
16	681.1	668.0	662.4	672

Table 2.1: Tangency Radii for AXUV

ments from setup to setup is well within the range of accuracy of the reconstructions. These measurements can therefore be trusted and used in interpreting the AXUV data.

The AXUV tangency radii are also useful for generating tangency radii for the core foil array. Since each of the four blocks of foil detectors are mounted at a known angle to the AXUV plate and the locations of the detectors on the blocks are fixed, we know the angles between all of the foil viewing chords and any of the diode viewing chords. With these angles and a measured R_A from one of the diode channels we get the R_A values for the foil detectors and can repeat the process described above to get their tangency radii.

Chapter 3

Spatial Radiation Profiles

3.1 Inversion Problem and Solution

The problem faced when using bolometer data to generate spatial profiles of the plasma emissivity is one of converting a line integrated power density to a volume emissivity [9]. The mathematical technique for recovering spatial information from line integrated data is often referred to as Abel inversion. Problems of this kind are common to the inversion of data from other plasma diagnostics and astrophysical observations so the basic technique is well developed.

3.1.1 Circumstances and Assumptions

The tokamak is circularly symmetric so the bolometer views, that is the lines of the integration are all chords. We will assume the plasma is toroidally symmetric so that the viewing chords can be treated as intersecting their corresponding tangency radii at the same toroidal angle. This means we also assume the radial emissivity profile we obtain is applicable all around the tokamak. Figure (3-1) shows the situation for a single chord.

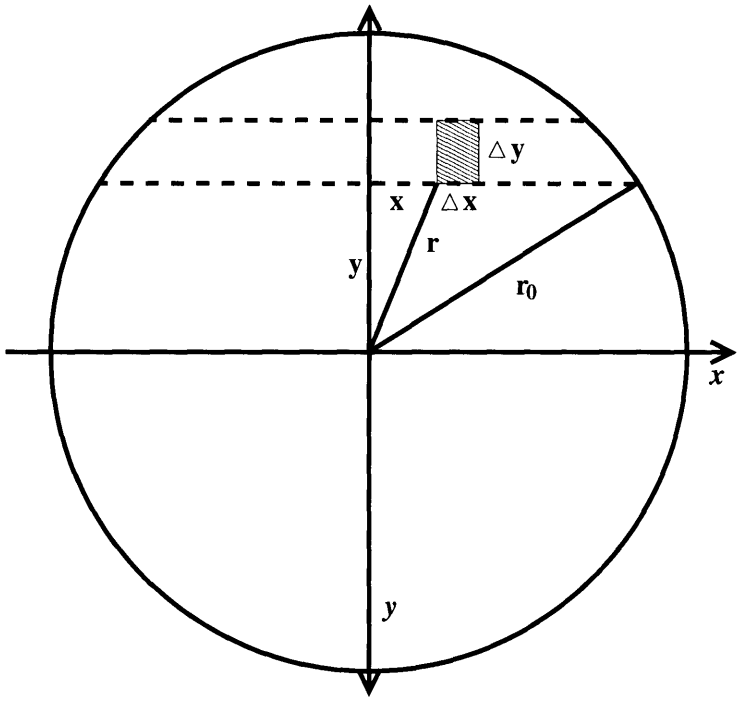

Figure 3-1: Diagram for a single viewing chord, bordered by dashed lines. (After-Bockasten 1961 [10])

3.1.2 Inversion

If we define $e(r)$ to be the volume emissivity in units of power per unit volume then the line integrated emissivity or brightness (in units of power per unit area) for the detector channel, which we will hereafter identify by its tangency radius (y in Figure (3-1)), is given by

$$b(y) = 2\int_0^{x_0} e(r)dx. \tag{3.1}$$

Since triangle xyr is a right triangle $x = \sqrt{r^2 - y^2}$,we can change equation(3.1) to an integral with respect to the coordinate of interest r.

$$b(y) = 2\int_y^{r_0} e(r)(r^2 - y^2)^{-\frac{1}{2}} r dr \tag{3.2}$$

Now we can use Abel's inversion to write

$$e(r) = -\frac{1}{\pi}\int_r^{r_0} \frac{db}{dy}(y^2 - r'^2)^{-\frac{1}{2}} y dy \tag{3.3}$$

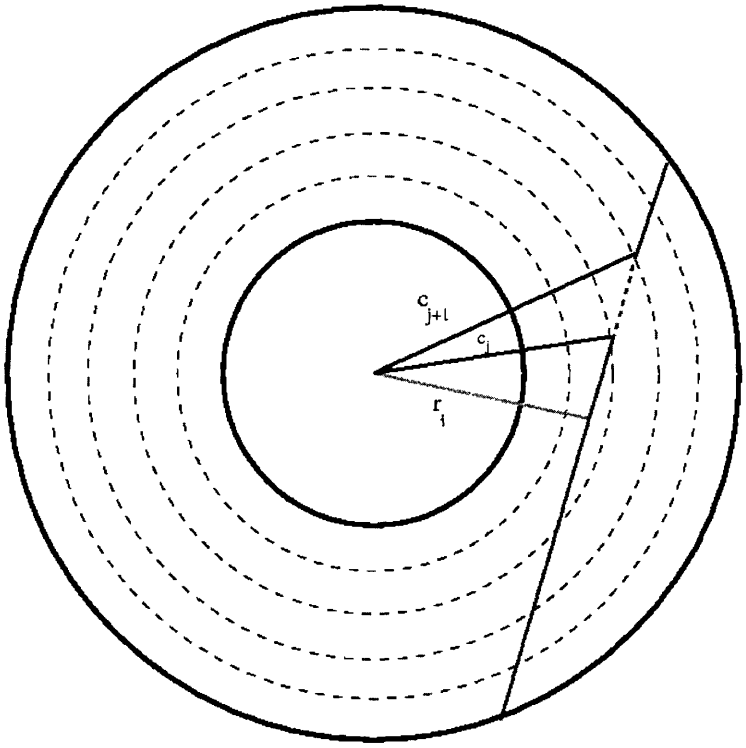

Figure 3-2: Diagram for a single chord. (Bockasten 1960)

$\frac{db}{dy}$ in this equation is known because we have several channels in the bolometer array. The continous variable equations discussed in this section cannot be applied directly to our bolometer data because we have a limited and discrete set of power measurements each of which may contribute differently to the complete profile.

3.1.3 Calculation

The actual calculation of the spatial emissivity profile is carried out using matrix methods. We begin the finite treatment of the inversion problem by defining a series of concentric circles separated by equal increments in radius as shown in Figure (3-2). We identify the j-th circle by its radius c_j. These radii constitute a set of radial coordinates onto which the inversion is mapped, corresponding to the coordinate r in the previous section. We can also label the tangency radius of the viewing chord of the ith detector by its length r_i. This is a discretization of the coordinate y in the previous section. The length of the portion of the i-th viewing chord between two

adjacent circles c_j and c_{j+1} is

$$S_{ij} = 2(\sqrt{c_{j+1}^2 - r_i^2} - \sqrt{c_j^2 - r_i^2}) \tag{3.4}$$

Figure (3-2) illustrates this. The factor of two is again present because equal portions of the viewing chord lie between the circles on both sides of the tangency radius. The rows of the matrix S are thus sets of discrete x coordinates and each row corresponds to a particular detector view. S is what relates the tangency radii of the detectors to our discrete coordinates.

Now that we have discretized versions of the various coordinates of the previous section we can rewrite the integrals found there as matrix products (matrices will be denoted by capital letters while lower case symbols stand for vectors). Equation(3.1)then becomes

$$b(c_l) = \sum_k S_{lk} e(r_k) \tag{3.5}$$

Finding the emissivity vector e is now a matter of inverting (3.5) subject to two conditions(the following comes from [11]). First, we want to have a minimal $(Se-b)^2$ so that we obtain the least-squares solution to our problem. Secondly, we wish to ensure the smoothness of E. We do this by adding a term proportional to the square of the second derivative of e, $(De)^2$, to the quantity we seek to minimize. Therefore, we want to minimize

$$K = (Se - b)^2 + \epsilon(De)^2 \tag{3.6}$$

where D is the discrete second derivative matrix given by

$$\begin{aligned} D_{i,i} &= -2 \\ D_{i,i-1} &= 1 \\ D_{i,i+1} &= 1, \end{aligned}$$

For arbitrary matrix A (either D or S in our case) we define $A^2 = A^T A$ and the

minimum is found by solving

$$\begin{aligned} 0 = \frac{dK}{de} &= \frac{d}{de}[(e^T S^T - b^T)(Se - b) + \epsilon e^T D^T De] \\ &= 2S^T Se + 2\epsilon D^T De - 2S^T b \end{aligned}$$

The solution is then given by

$$(S^T S + \epsilon D^T D)e = S^T b \tag{3.7}$$

Now let's define a matrix M as follows to simplify the expression of the final inversion

$$M = S^T S + \epsilon D^T D \tag{3.8}$$

A singular value decomposition is carried out numerically to obtain a diagonal matrix W such that

$$M = UWV \tag{3.9}$$

with W a diagonal matrix and U and V mutually orthogonal. The pseudo-inverse matrix used to obtain the solution to the matrix equation is then

$$M^{-1} = VW^{-1}U^T \tag{3.10}$$

where W^{-1} is the same as W with the nonzero values (the singular values) replaced by their reciprocals. Finally, the emissivity is just

$$e = M^{-1}S^T b \tag{3.11}$$

where e is a vector of volume emissivities at the radial data points at the recorded times and b is a vector of line intergrated emissivity or brightness readings from each of the bolometer viewing chords, again at discrete time points. This is the linearized, matrix form of Equation (3.3) from the previous section.

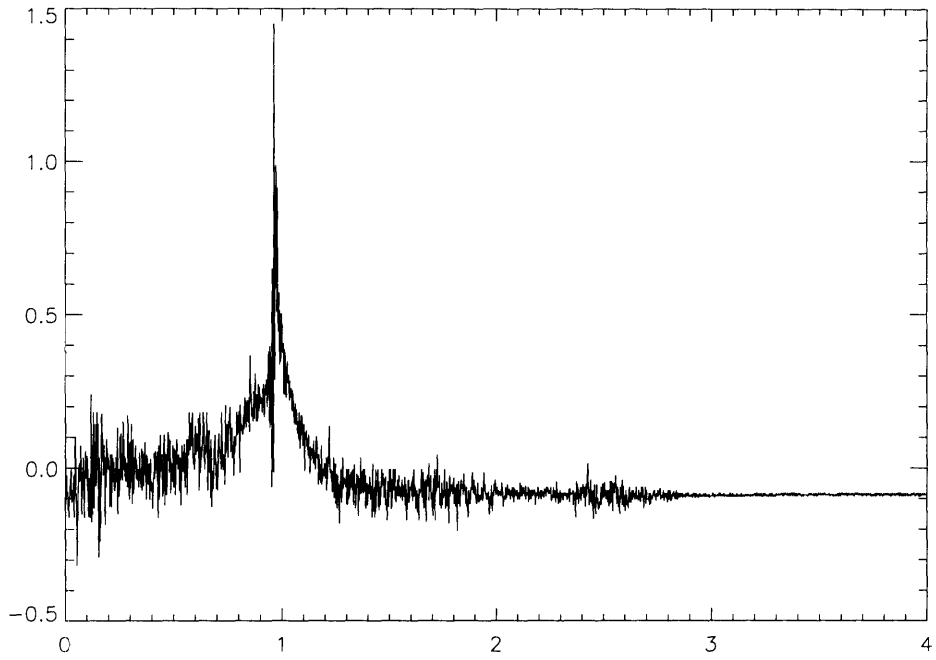

Figure 3-3: The signal from a single channel.

It is easiest to see from the matrix form of the calculation that to obtain the emissivity at some radius we add up the powers absorbed by the detectors with the contribution of each weighted by how much of the detector's viewing chord is in the region corresponding to the radius of interest.

The raw output of a single detector channel typically looks like Figure (3-3). This raw signal (V_s) is related to the power absorbed by the detector channel P_{abs} by the equation

$$P_{abs} = (V_s + \tau_c \frac{dV_s}{dt})) \frac{1}{V_{in} S} \tag{3.12}$$

where V_{in} is the input voltage amplitude across the detector bridge and τ_c and S are the quantities calculated as part of the calibration of the detector (see Chapter 2). This P_{abs} absorbed by a detector channel is proportional to the radiated power absorbed by a unit of area facing the plasma directly because the measured voltage is, as discussed in Chapter 2, proportional to the temperature change in the detector. The radiated power absorbed by the detector is given by.

$$P_{abs} = \frac{Et \cdot b}{4\pi} \tag{3.13}$$

Et in this expression is the etendue of the detector channel, given by

$$Et = \frac{A_{ap}A_d}{l^2} \tag{3.14}$$

where A_{ap} is the area of the aperture in the bolometer box,A_d is the effective aperture due to the size of the bolometer detector foil and l is the distance between. We can see that dividing P_{abs} by Et gives the correct units for b.

As can be seen from Figure (3-3) the measured voltage signal V_s is quite noisy. Taking the derivative of the signal, as is necessary to obtain P_{abs} magnifies the noise so that simple local average smoothing is not enough to suppress it. The noise filtering technique used for the Alcator foil bolometer array data is a procedure called Lee filtering which makes use of the local statistics of the measured signal. The filtering algorithm was developed for use in suppressing speckle noise in satellite images [12]. The equation for the filtered signal y in terms of the measured signal z is

$$y = \bar{y} + \frac{var(y)}{\bar{y}^2\sigma_v^2 + var(y)} \tag{3.15}$$

where

$$var(y) = \frac{var(z) + \bar{z}^2}{\sigma_v^2 + 1} \tag{3.16}$$

and $var(z) = z/(n-1)$ and all averages are taken over $2n-1$ data points. The smoothing is applied both to the measured voltage and its derivative but the smoothing must be carried out over a larger time window (about twice as large) for the derivative. For the C-mod foil bolometer array the time window is 40 milliseconds. The effect of the filtering procedure can be seen by comparing Figure (3-3) to Figure (3-4).

Following this procedure for each detector channel we can obtain a brightness profile like the one shown below in Figure (3-5). The brightnesses from the different chords can now be inverted as described above, following Equation (3.11) to give the volume emissivity profile we are after which is shown here.

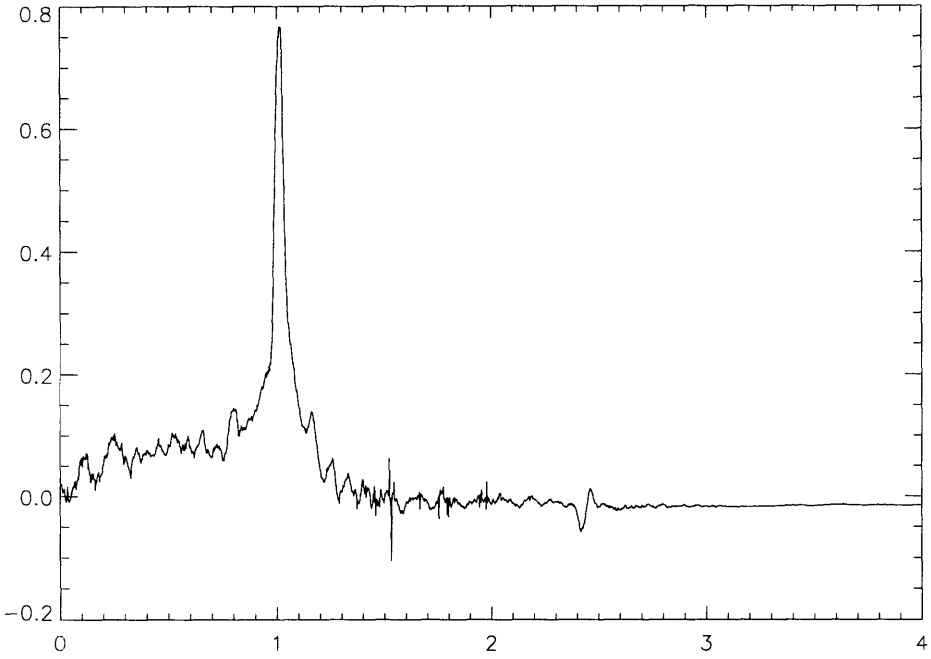

Figure 3-4: The Lee filtered signal from a single channel.

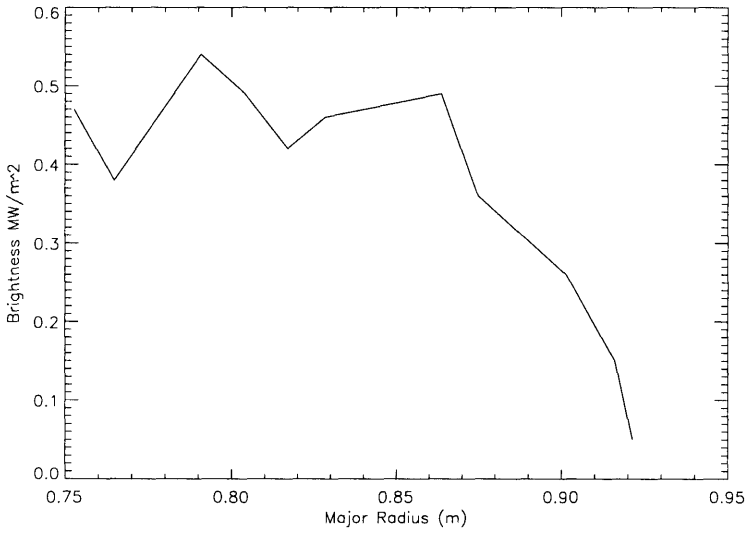

Figure 3-5: Brightness Profile

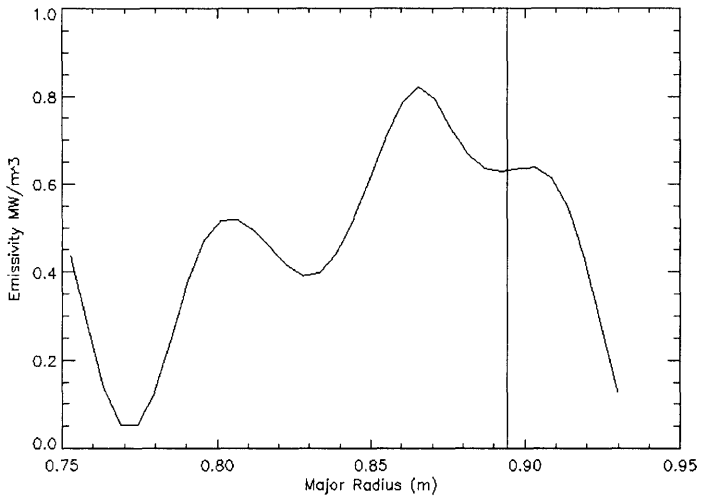

Figure 3-6: Emissivity Profile

3.2 Sources of Error

There are two main sources of error in the radiation profile as measured by the foil bolometer array: the voltage offset and the noise in the detector and associated electronics.

3.2.1 Detector Voltage Offset

In addition to varying from channel to channel as one would expect the voltage offset of the various channels also varies from shot to shot and linearly within shots (see Figure (3-7)). We try to remove this offset as the data is analyzed by subtracting a linear fit to the averages of the first few and last few time points where no real data is taken. We denote regions where no data is available from the plasma with negative times. Unfortunately, there is still uncertainty in the calculation of the magnitude of the offset which must be included in the error.

3.2.2 Detector Noise

Figure (3-3) also shows that the signal from the bolometer bridges is subject to a good deal of random noise. Even with reasonable binning and smoothing of the data

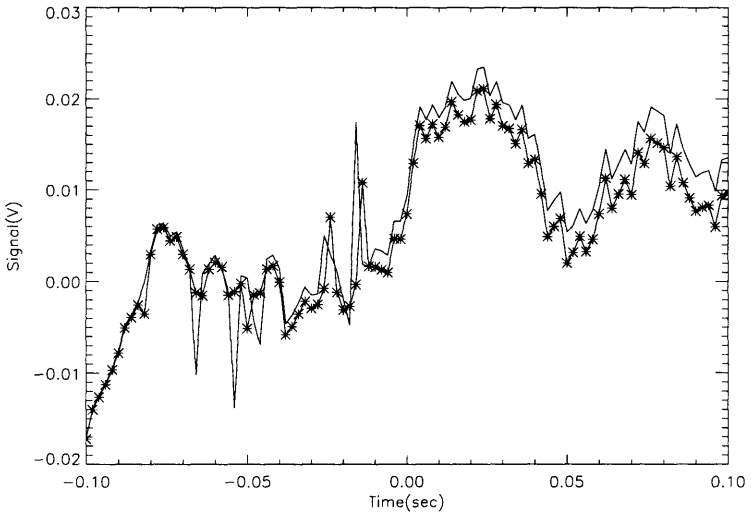

Figure 3-7: No marking: Signal; Stars: Signal with approximate offset subtracted.

the errors of the line integrated powers are about 15%. These errors have different effects depending on the channel they occur in as discussed in the next section.

3.3 Error Sensitivity

The errors in the line integrated data must be propagated through the inversion process to give proper error estimates in the final profile.

3.3.1 Relative Sensitivity of the Channels

It turns out that error accumulates as one probes deeper into the plasma [13] and the accuracy of profile data is more susceptible to errors in the signals from the innermost viewing chords of the bolometers. Figure (3-8) shows that at the same fractional error in input signals the inner viewing channels have much larger errors. Notice how insignificant the error due to the outermost channel is compared to the nearly 50% error resulting from the same detector error in the innermost channels. The next two figures show the result of this high sensitivity of the inner channels for the final profiles.

Figures (3-9) and (3-10) illustrate the the significant differences in the effect of

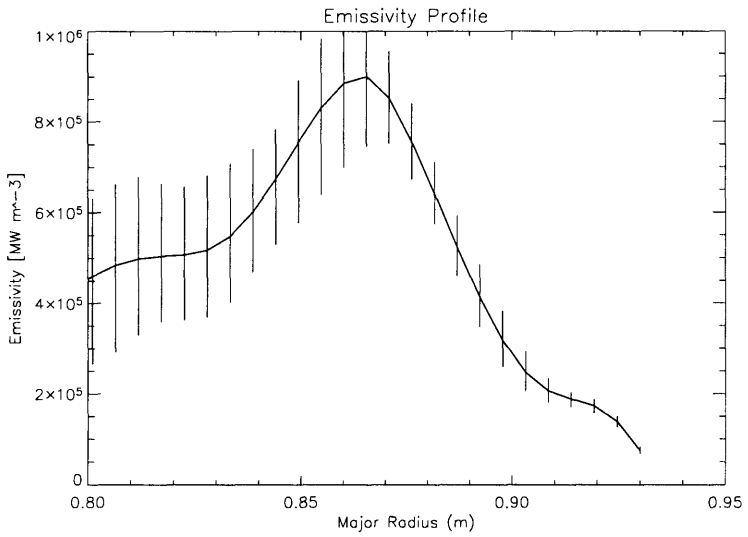

Figure 3-8: The fractional error of all channels was 10% in this demonstration.

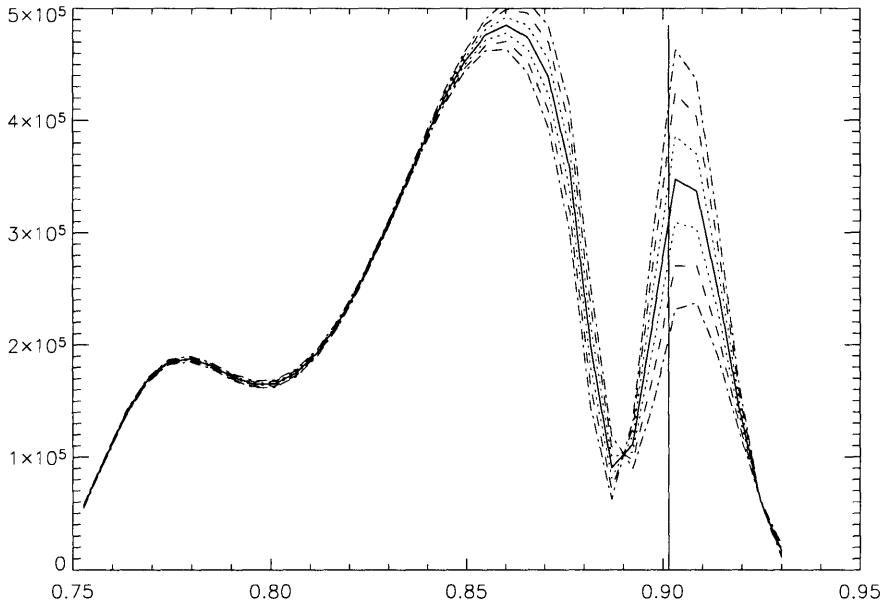

Figure 3-9: Outer Channels: Errors of 10,15, and 20%

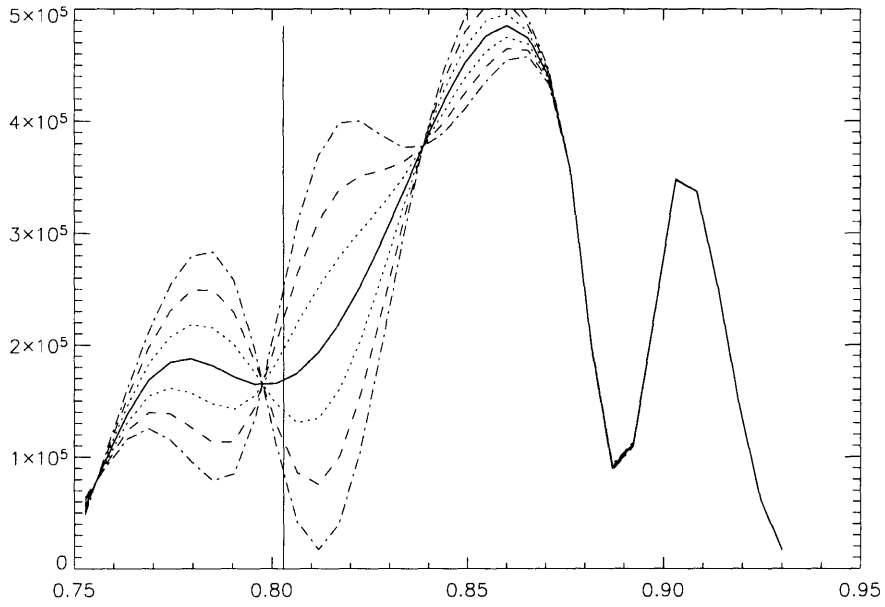

Figure 3-10: Inner Channels: Errors of 10,15,and 20%

errors on inner channels compared to errors on outer channels. In Figure (3-9) we see that errors in outer channels do not have a strong effect on the overall shape of the profile. In contrast, Figure (3-10) shows the drastic effects of similar errors on emissivity profile shape when the errors occur in a channel just ten centimeters closer to the plasma core. Hopefully, these examples have demonstrated the nature of error propagation in an Abel inversion.

The emissivity profiles discussed here can be used to recover the plasma radiation as it is measured by the 2π bolometers. The radiated power absorbed by the 2π foil is given by an expression like (3.12). An approximation (which assumes poloidal and toroidal uniformity of radiation) for the power radiated in the detectable range is then given by

$$P_{2\pi} = P_{abs,2\pi} \frac{A_{wall}}{A_{2\pi det}} \tag{3.17}$$

where $A_{2\pi det}$ is the area of the 2π detector foil and A_{wall} is the inner surface area of the tokamak. A reconstruction from the array data can serve both to provide new information about the plasma and as a check of our calibrations and calculations. Comparisons of this kind are discussed in the next chapter.

Chapter 4

Some Results

4.1 Overview

The results to be discussed in this thesis are of two categories: measurements of plasma radiated power and measurements of the plasma emissivity profile. As mentioned at the end of the previous chapter radiated power measurements can be obtained both from the bolometer arrays used to generate emissivity profiles and the 2π foil and diode bolometers. Results of this kind help us to determine how much energy is being lost from the plasma via radiation under various conditions. In this chapter one thing we will examine is how good the different bolometers are at providing a measurement of this radiation as well as the conditions under which it differs significantly (e.g. when impurity concentrations are high). Emissivity profiles gathered using the bolometer arrays tell us where in the plasma the radiation is chiefly coming from. We use this information on the local emissivity values together with information about local plasma properties obtained with other diagnostics to try to identify the main sources of radiation in the plasma. Examples of this kind of work which will be discussed in this chapter include using temperature profiles with the emissivity profiles and known temperature-line emission curves of different species to identify the main radiating species and determining the effect of the presence of a temperature/density pedestal on the emissivity profile.

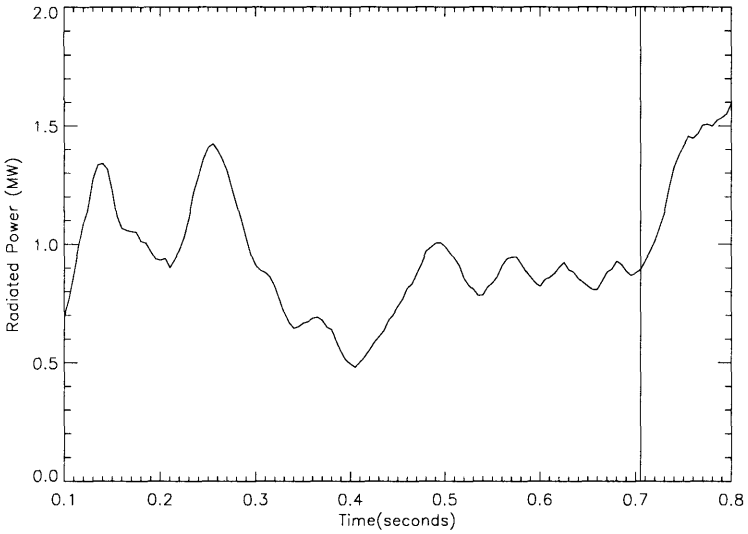

Figure 4-1: Foil Array Radiated Power

4.2 One-Hundred Percent Radiated Power

When the plasma has a high impurity content we expect that all of the power input will be radiated away. Under these conditions we can try to calibrate the bolometer diagnostics (in fact there are not many other practical options for calibrating the diode bolometers). Figure (4-1) shows the radiated power trace for a shot with impurity injection. The time of the last impurity injection (which brings the impurity concentration up to its final value before disruption) is shown as a vertical line on the trace.

The next Figure (4-2) shows the time traces of the radiated power obtained from the foil array and the two pi foil bolometer, along with the plasma current and average density which are important in determining the radiated power, for the same shot.

The fraction of the total input power radiated for the same shot is shown in Figure (4-3) for the segment of time following the final impurity injection. As shown in Figure (4-3) the bolometer array measures 100% radiated power fraction for this shot (accurate to about 5%) before disruption, as expected. For the plasma shown the power input was entirely ohmic and the impurity injected was argon. Similar results were obtained with a neon injection.

To determine the validity of this result the radiated power fraction as measured by

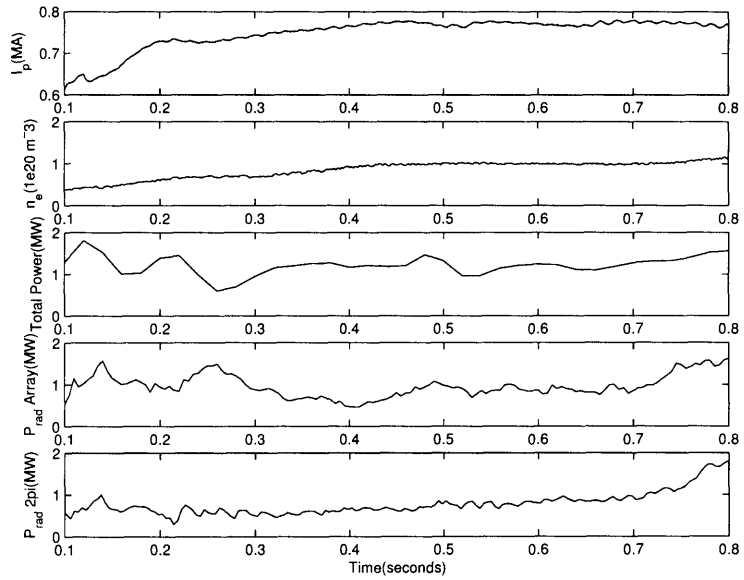

Figure 4-2: Plasma Properties and Radiated Powers

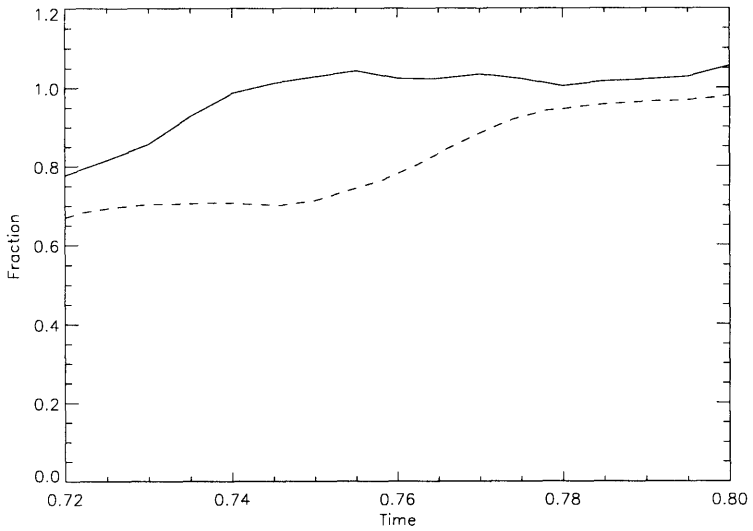

Figure 4-3: Radiated Power Fractions for the Foil Array (solid) and 2π (dashed) Bolometers

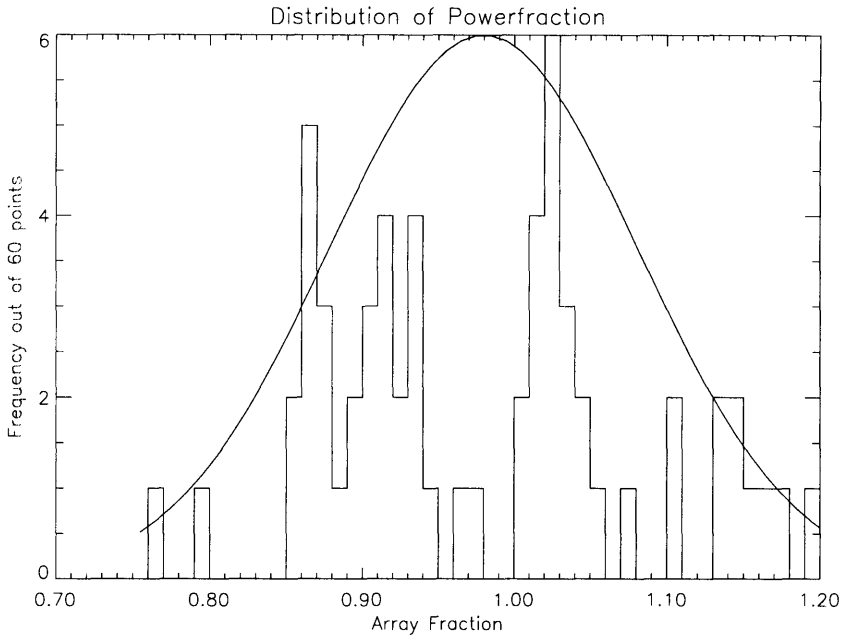

Figure 4-4: Array P_{rad} Fraction Histogram

Toroidal Field	5.4 T
Average n_e	1.5 $10^{20} m^{-3}$
Average T_e	1.5 keV
Average I_p	.78 MA

Table 4.1: Parameters for Figures 4-4 and 4-5

both the foil array and the 2π foil detector were determined at multiple time points on several shots with maximum radiated power. The results are shown in histogram form in Figures (4-4:Array) and (4-5:2π).

For shots for which 100% radiation is expected the radiated power fraction reconstructed from the foil array bolometer data averages 98% with a standard deviation of about 10% and a range of +/-20%. The values obtained from the 2π foil for the same shots average 100% with a 16% deviation and a +/-20% range.Table 4.1 shows relevant data for the shots used to generate the histogram plots.

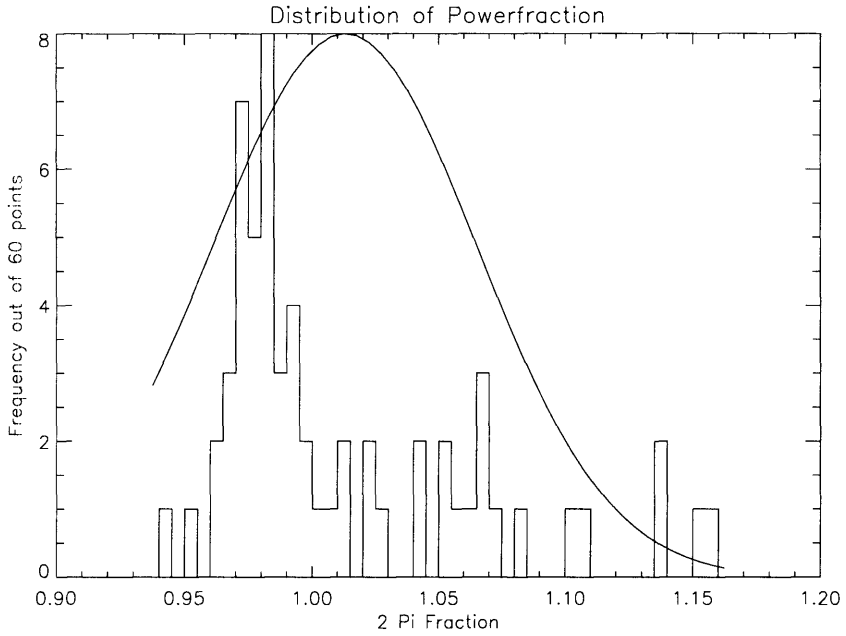

Figure 4-5: 2π P_{rad} Fraction Histogram

4.2.1 Effect of RF Input on Power Fraction

In this section we will cover the attempt to determine what changes in radiated power fraction, if any, result from increasing the input of RF heating power to the plasma. We will also study the effect of the plasma mode on the way radiated power responds to total input power. The results shown in Figure (4-6) were obtained by averaging the radiated power fraction data from several instances with the desired input RF power. Data from both foil array reconstruction and the 2π foil bolometer are plotted.

Figure (4-7) is similar to Figure (4-6) except that in this case the radiated power output is plotted against the input power due to both ohmic and radio frequency heating.

Table 4.2 shows the average plasma conditions (prior to RF input) of the plasmas from which the power data for the figures was taken.

4.2.2 Discussion

Both plots show that radiated power increases with increasing input power, which is expected since the plasma temperature should rise as the power increases. We can

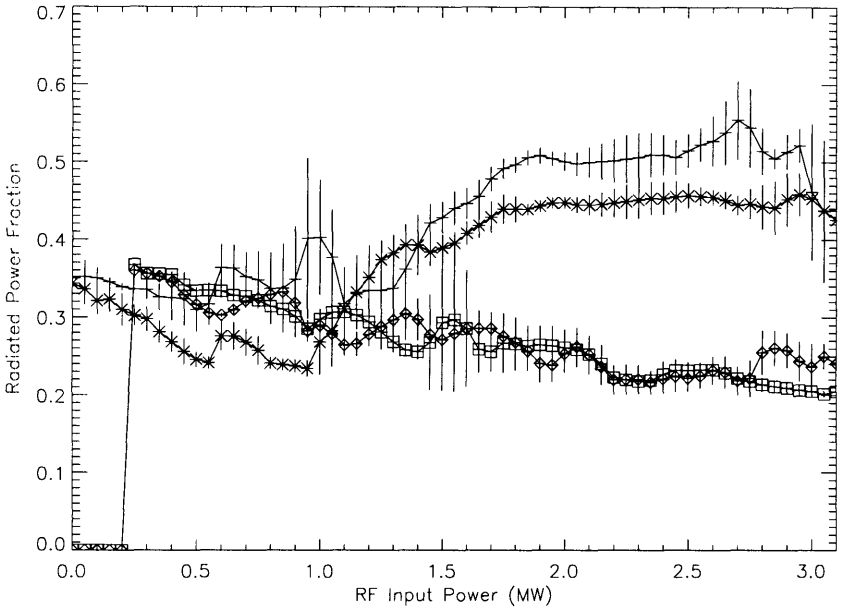

Figure 4-6: Radiated Power Fraction vs. Input RF Power

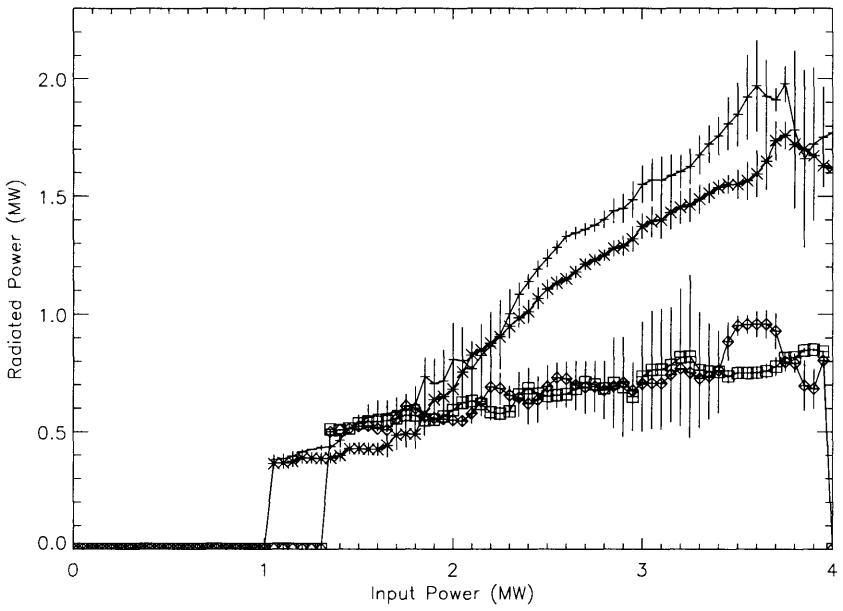

Figure 4-7: Radiated Power Fraction vs. Input Power
For Figures 4-6 and 4-7; No Marking: Foil 2π (H-mode), Stars: Foil Array (H-mode), Diamonds: Foil 2π (L-mode), Squares: Foil Array (L-mode).

Toroidal Field	5.4 T
Average n_e	.9 $10^{20} m^{-3}$
Average T_e	1.5 keV
Average I_p	.79 MA

Table 4.2: Parameters for Figures 4-6 and 4-7

also see that the plasma radiates more when in H-mode than when in L-mode. H-mode is a high confinement mode in which a transport barrier develops in the plasma edge leading to an increase in the plasma density and a doubling (approximately) of the confinement time. The actual ratio of the energy confinement time after the transition to H-mode to the confinement time before is called the H factor. One feature of H-modes which is significant for our discussion is that they do not occur below a threshold input power (see more about H-modes in e.g. [3]. Figure (4-7) shows that data from shots that at some point have an H-mode match the data from shots that remain in L-mode for their duration when input energies are too low to produce an H-mode. Figure (4-7) also give us a better handle on the difference in radiated power between H-mode and L-mode plasmas. We can see that in both cases the radiated power scales linearly with input power. The difference is that in H-mode the plasma the radiated power rises with input power about three and a half times as fast as in the L-mode case. The reason for the power difference would not be so clear from Figure (4-6) alone.

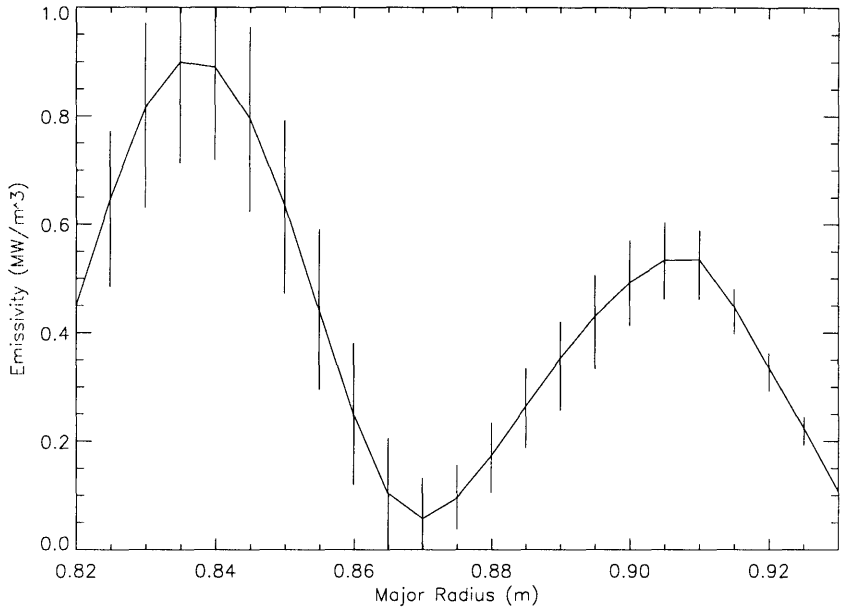

Figure 4-8: Standard Shot Emissivity Profile

Toroidal Field	5.4 T
Average n_e	.9 $10^{20} m^{-3}$
Average T_e	1.5 keV
Average I_p	.79 MA

Table 4.3: Parameters For Figure 4-8

4.3 Emissivity Profiles

Typical emissivity profiles for unmodified, ohmically heated plasmas in Alcator C-mod look like the one shown in Figure (4-8).

The main, consistently reproduced features in deuterium plasmas without intentional injection of impurities are a strong peak at R=0.85 m and a minimum at R= 0.87 -.89 m. Emissivity values at the minimum are usually about a tenth the magnitude of the maximum emissivity. Sometimes the reconstruction of the emissivity profiles returns negative emissivity values. This is an unphysical result and must be accounted for. The problem arises because the reconstruction of the emissivity profile assumes a plasma that is always everywhere transparent to the radiation of interest, and this is not the case for the real plasma. The general properties of shots like this

one are common on C-mod. We will therefore be able to select similar shots so that the features of their emissivity profiles may be compared. It should not be assumed that emissivity profiles like Figure. (4-8) represent the results for a pure plasma. Profiles like this merely offer a kind of baseline for further comparison. There are many impurities present, probably most important are carbon and molybdenum which radiates strongly, not being completely stripped of electrons until reaching temperatures a few times greater than those achievable in C-mod. In this section we will look at the effects of adding various species of impurities (including larger than average quantities of boron) to the plasma. We will also examine the effect of the varying the location of the ion cyclotron resonance on the emissivity profile of the plasma. We will also attempt a study of the effect of internal transport barriers on the emissivity profile.

4.4 Impurity Species

The effect of different impurity species on the emissivity profile was checked by comparing shots similar in all respects except injected species. Shots with injections of helium, argon, and neon are compared to shots with an injection of the plasma majority species (deuterium). Note that all of these data come from L-mode shots without RF heating. Figure (4-9) shows the results of this comparison, along with the errors on the profile (corrected for radial position). The results are discussed in detail below.

Toroidal Field	5.4 T
Average n_e	.9-1.0 $10^{20}m^{-3}$
Average T_e	1.3-1.6 keV
Average I_p	.8 MA

Table 4.4: Parameters for Figure 4-9

Helium

Shots with an injection of helium have emissivity profiles very similar to shots with only the majority species injected, so much so that it is not possible to tell solely from

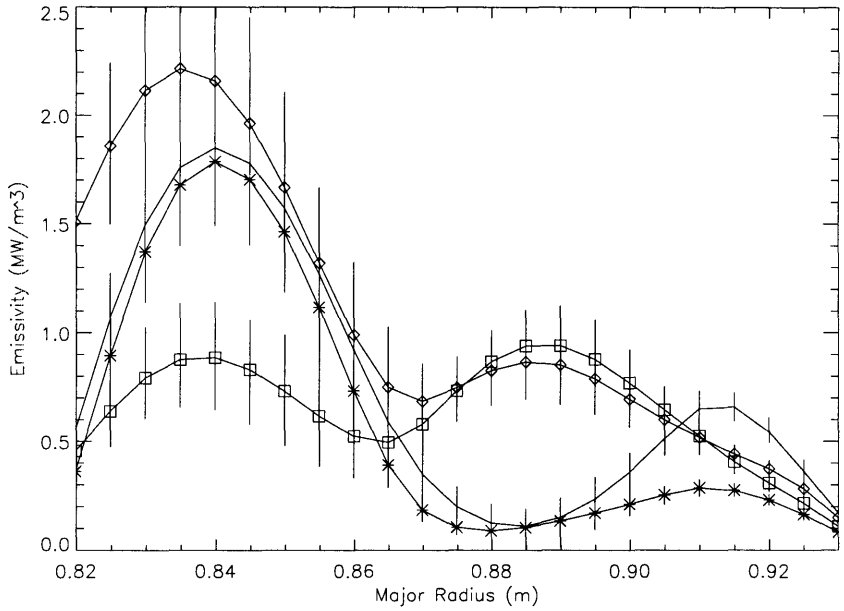

Figure 4-9: Multiple Injected Species: No marking: D; Star: He; Square: Ne; Diamond: Ar

the profiles when the helium was injected (we'll see later that this is not the case for other injected impurities). The observable difference in shots with a helium injection is that the emissivity in the scrape-off layer (separtrix is at R=.89m) is depressed when compared to the emissivity further in. This suppression of edge emissions is sustained through the duration of the helium gas puff. It is not clear whether this suppression corresponds to an increase in radiation from further in the plasma. However, as we can see from Figure (4-9) there does not seem to be increased emissivity in the region of highest emissivity in shots with deuterium injection.

Neon

Neon injection shots show a prominent peak in emissivity in a region associated with diminished emissivity in deuterium injection shots. This feature of neon injection shots as compared to deuterium shots is well outside the error range of the emissivity profiles. Another feature of neon shots that is clearly visible in Figure (4-9) is that the main emissivity peak decreases. Since this feature occurs deeper in the plasma it is not as clear that it is not accounted for by the error in the emissivity profile. The

decrease in emissivity at the inward emissivity peak is repeated in various shots and over whole durations of neon puffing so we may be confident that it is not an artifact.

Argon

The puffing of argon gas into the plasma has an effect similar to the addition of neon. An emissivity peak emerges in a region that is associated with reduced emissivity in unmodified and deuterium injected plasmas. Unlike neon shots the inner emissivity peak is, if anything, increased rather than diminished. This increase along with the apparent slight inward shift of the peak visible for the particular case shown are not strong enough or consistent enough to overcome the errors in the measurement. It is therefore not possible to distinguish neon and argon injection shots on the basis of snapshots of the emissivity profiles.

Discussion

Now we must see if we can make sense of the experimental observations presented so far. As discussed in Chapter 2, the foil bolometer array "sees" radiation in the vacuum ultra-violet and soft x-ray ranges. This means that it is sensitive to the line radiation due to all the transitions of the lighter impurities. These impurities do not radiate in the core of the plasma, being completely stripped of their electrons at tokamak core temperatures. Such impurities,particularly neon, have been suggested as a means of uniformly dispersing the plasma's heat in the edge while avoiding excessive radiation from the core. Assuming, as we have, that differences between the emissivity profiles of shots with an injected impurity and shots without are due solely to the impurity we are left with the question of how the impurity got to where it is radiating from.

This brings us to the problem of impurity transport in a tokamak plasma. This problem is treated in [14] and in great detail in [15] the following borrows heavily from both of these. We can begin by writing down the classical (collisional/cylindrical plasma) equation for radial (majority species) ion flux

$$\Gamma_i = -n_i D_i \left(\frac{1}{p_i}\frac{dp_i}{dr} - \frac{T_Z}{ZT_i}\frac{1}{p_Z}\frac{dp_Z}{dr} - \frac{3}{2}\frac{1}{T_i}\frac{dT_i}{dr} \right) \tag{4.1}$$

where the subscripts i and Z refer to the majority and impurity species respectively and n,p,and T are the density,pressure, and temperature. Z by itself is the charge of the impurity ion. Note that the second term of Eqn. 4.1 is negligible. The diffusion coefficient for this flux is

$$D_i = \frac{T_i}{m_i \omega_{ci} \tau_{iZ}} \tag{4.2}$$

where τ_{iZ} is the $i \rightarrow Z$ collision time

$$\tau_{iZ} = \frac{12\pi^{3/2}}{2^{1/2}} \frac{m_i^{1/2} T_i^{3/2} \epsilon_0^2}{n_Z e_i^2 e_Z^2 ln\Lambda} \tag{4.3}$$

We can now obtain the impurity flux Γ_Z from the majority ion flux (Eqn. 4.1,the ambipolarity condition

$$\Gamma_i - \Gamma_e + Z\Gamma_Z = 0 \tag{4.4}$$

and the fact that Γ_e scales like

$$\frac{m_e n_e \nu_{ei}}{m_i n_i \nu_{iZ}} \approx \frac{n_i}{n_Z Z^2} \left(\frac{m_e}{m_i}\right)^{1/2} \tag{4.5}$$

which is small in a fusion plasma. For our purposes the important thing to note is that Γ_i and Γ_Z are of opposite sign. This means that as the majority species moves out from the core the impurity moves in. The (flux surface averaged) diffusion equation for the neoclassical case is the same as Eqn. 4.1 with different coefficients on the terms, notably a factor of $\approx q^2$ multiplying the whole expression with q the safety factor. There is also a neoclassical convective drift velocity v_{neo}, or pinch. Finally, it is known that real particle transport happens faster than the predictions of neoclassical theory allow. On other toroidal experiments which have facilities to carry out fast spectrally resolved measurements of plasma radiation in the VUV range experiments have been carried out to determine D and v_{neo} [16] but the results disagree even as to whether neoclassical values are good enough for the lighter impurities (e.g. Ne and Ar). Fast VUV spectrometers are necessary for such measurements because we want to know how much of the impurity is in what charge state. The charge state appears in the diffusion coefficient via the collision time τ_{iZ} (Eqn. 4.3).

Work done to model the emissivity profiles for individual species in support of the transport research described above is useful for interpreting our results as well. Based on the work of Beil et al. [16] it seems that on argon injection shots the additionaly peak in emissivity is due to Ar-XVI, Ar-XV, and Ar-XIV charge states.

An alternative, or more likely contributing, explanation for the observed changes in emissivity profiles measured with the foil bolometer array is the local variation of some plasma parameters in response to the impurity injections. Impurity injections directly change the plasma density and temperature profiles (just by radiating in the edge region they change the temperature profile), which in turn must affect the emissivity profile (see Eqn. 1.14). These changes, and the change in Z_{eff} which must accompany any significant impurity injection are usually taken to be of secondary importance.

4.4.1 Boronization

To improve performance the Alcator C-mod tokamak is periodically boronized, that is its inner surface is coated with a thin layer of boron. Immediately after boronization it can be expected that a significant amount of boron enters the plasma from the wall. To see the effect that this boron has on the emissivity we compare averaged profiles from shots separated from a boronization by a different number of run days. The results are plotted in Figure (4-10). Although the profiles come from different boronizations they were all taken from ohmic L-mode shot segments. The average properties of the shots are displayed in Table 4.5.

Toroidal Field	5.4 T
Average n_e	.94 $10^{20} m^{-3}$
Average T_e	1.5 keV
Average I_p	1.0 MA

Table 4.5: Parameters for Figure 4-10

One thing that is immediately clear is that the post-boronization profile closely resembles the profile I have presented as a "standard" shot. Much more so than the

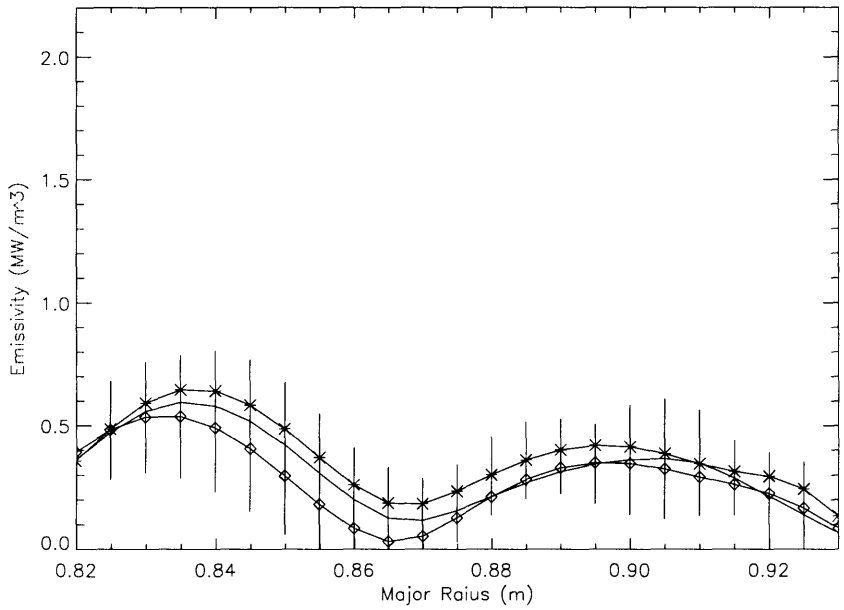

Figure 4-10: Profiles: No marking: Pre-Boronization; Star: 5 Runs Post-Boronization; Diamond: 9 Runs Post-Bornization

pre-boronization shot. This turns out not to be so surprising because profile shown in Figure (4-8) was from a day right after a boronization (different from the borinization resulting in the present profile). This is not a problem for the comparisons we have used so far nor for the next section because all of these profiles were taken from shots within three days of some boronization so we would want to allow for boronization effects anyway. Figure (4-10) shows that there were no observable changes in average profile from one boronization to another that did not fall within the errors on the measurements. We know that plasma Z_{eff} is strongly affected by boronization so these results may show that effects on radiated power do not last long at all. It should be pointed out that unlike the injected impurities discussed in this section there is a steady source of boron throughout entire shots, except during disruptions.

4.4.2 ICRF Resonance Position Variation

Ion Cyclotron Resonance Frequency heating deposits power into the plasma at a resonance layer in the plasma (see e.g. [17] for more on RF heating). We can study the effect of changing the resonance location by using shots with different on-axis

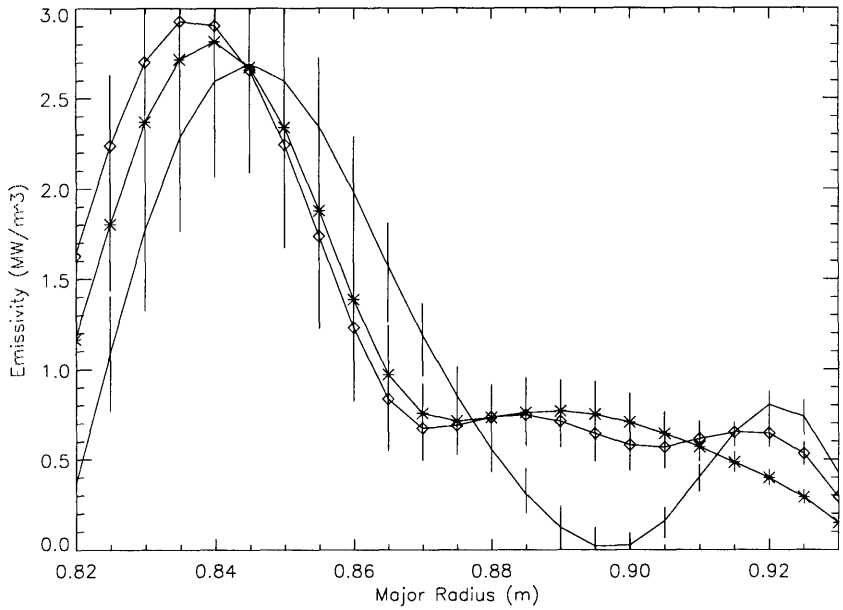

Figure 4-11: Resonances: No marking: On-axis; Star: Low field side; Diamond: High field side

Average n_e	1.0 $10^{20}m^{-3}$
Average T_e	1.45 keV
Average I_p	.8-1.0 MA

Table 4.6: Parameters for Figure 4-11

toroidal magnetic field strengths. Average emissivity profiles for shots with resonances at three different locations is shown in Figure (4-11) all with 2.3MW of net RF power at 80MHz. Prior to this investigation it was unknown whether changing the resonance position would have any significant effect on the emissivity profiles of Alcator C-mod plasmas. Further average properties of the plasmas are recorded in Table 4.6

We start by identifying the salient features of the emissivity profile in shots with on-axis RF heating. Two distinct examples of on-axis heated shots are provided by the profiles without special symbols on the plots in this section and the similarly unmarked profile in Figure (4-12) of the next section. These profiles show what is common to D plasmas without RF heating (see Fig. (4-8)). The profile shape is similar to the one already seen in ohmically heated deuterium plasmas with the main difference being a broadened and intensified primary peak in emissivity resulting in an

outward displacement of the emissivity minimum. Figure (4-11) shows that profiles for high field and low field shots are virtually identical to each other within the error of the measurement but are substantially different from the profile of a shot with on-axis heating. Specifically both profiles from shots with off-axis ion cyclotron heating seem to show an overall inward shift of the emissivity. This behavior cannot really be confirmed in the main emissivity peak because of the large errors deep in the plasma. The high emissivities in a region where low emissivity is expected in shots with on-axis heating are unmistakable though. These results demonstrate that the location of the ion cyclotron resonance, at least whether it is on- or off-axis has a moderately significant effect on the shape of the emissivity profile.

4.4.3 Revisiting an Impurity

Armed with the information we now possess about the behavior of deuterium plasmas when subject to ion cyclotron heating we can return to an injected impurity we ignored until now. Lithium is injected into the plasma in the form of a single pellet which is ablated and dispersed. Lithium probably should not show up in emissivity profiles as it is a quickly ionized low-recycling species which should leave the plasma after not much longer than the foil array detectors' time resolution. The reconstructed radiated power measurements do not show a response to the addition of Lithium. Figure (4-12) compares an average emissivity profile of shots with RF heating and lithium to a shots without lithium. The deformation (compared to the lithium-less shots) of the emissivity peak to include a lump to the outboard side is similar to but not quite the same as the behavior of shots with argon and neon injections. This feature is sustained throughout the application of RF heating, raising the suspicion that it may be an artifact of the heating after all. The feature in the lithium profiles may be left over neon as that gas was injected close to the Li pellet shots.

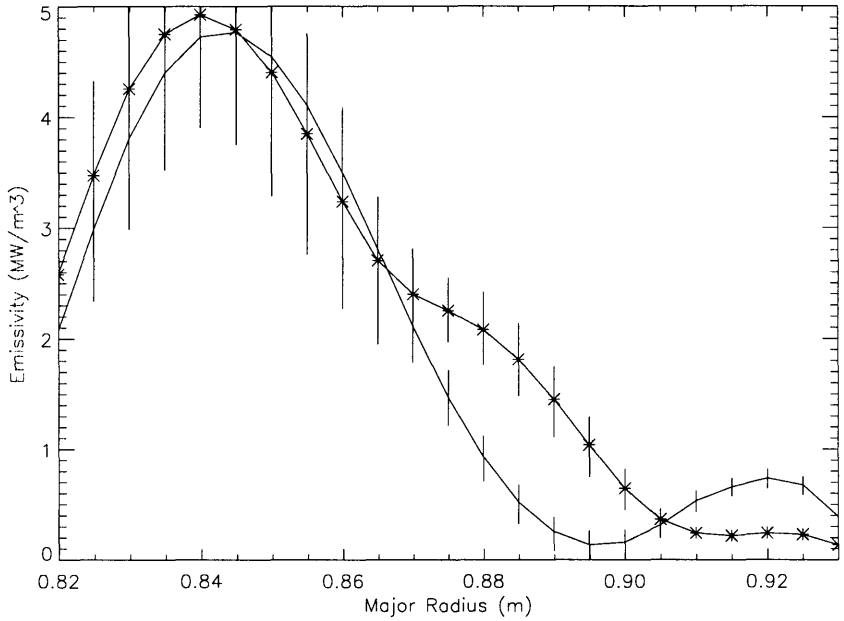

Figure 4-12: Profiles: No marking: Deuterium; Star: Lithium

4.4.4 ITB Effects

The information about off-axis ion cyclotron heating also frees us to investigate the emissivity profiles of plasmas with internal transport barriers (ITBs). These barriers are produced using off-axis heating. Following the discussion about impurity transport, we can perhaps expect that an alteration in the transport properties of the plasma will result in a change in the emissivity profile. Figure (4-13) is a comparison of emissivity profiles showing a plasma with RF heating and no ITB and a plasma with RF heating and a double barrier ITB. Both profiles are from shots with argon injected.

Table 4.7 shows the average data for the shots used to generate Figure (4-13). Note that the on-axis field is higher than usual, resulting in an off-axis RF resonance location. The presence of RF heating also explains the higher average temperature for these shots.

There are a couple of possibly important differences in plasma condition between the two cases shown. First, the heating in the non-ITB case is on-axis while the heating in the ITB case is off-axis. Secondly, the RF heating power is about .5MW greater

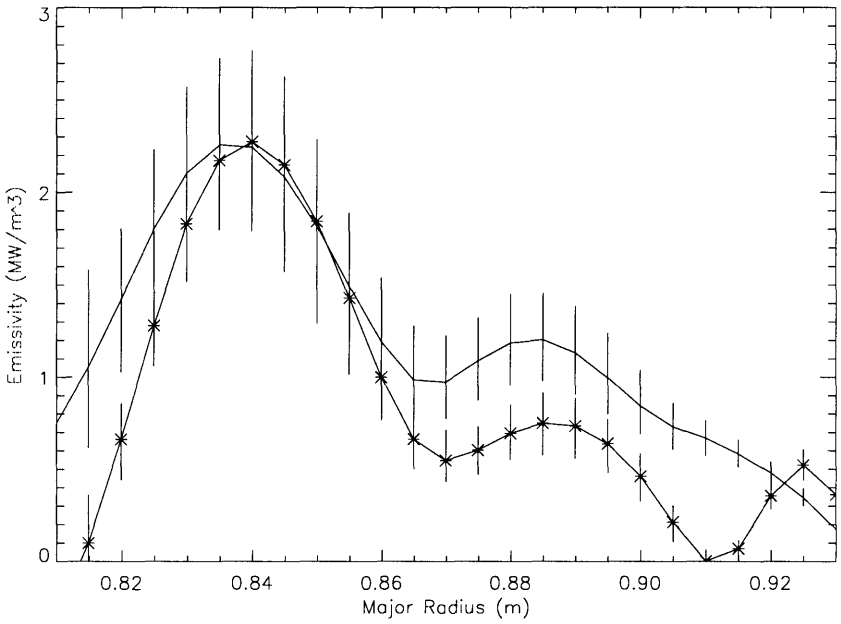

Figure 4-13: Profiles: No marking: No ITB; Star: ITB

Toroidal Field	6.4 T
Average n_e	1.0 $10^{20} m^{-3}$
Average T_e	1.85 keV
Average I_p	.8 MA

Table 4.7: Parameters for Figure 4-13

in the non-ITB case. There is, however, only one significant difference between the profiles. The second minimum in emissivity, occuring in the pictured case at R=.91, is common to most of the ITB plasmas studied but appears to be unique to them. This seems to be a real, if small, effect but it is difficult to explain. The minimum in emissivity appears to occur a full centimeter out from the density/temperature pedestal possibly due to a lack of spatial resolution. [Additionally the emissivity begins its drop further in.]

4.5 Impurity Identification by Temperature Profile

When impurities like neon or argon are intentionally injected into the plasma we can be fairly certain that the majority of the radiation is due to that impurity. When the contamination of the plasma is not intentional identifying the species responsible for most of the radiation is more problematic.

One approach is to use the temperature profile of the plasma together with its emissivity profile. This approach to identifying the main contributor to plasma radiation is based on the fact that different species have strong radiation peaks at different temperatures [18]. Plasma temperature profiles are available from Thomson scattering and ECE diagnostics. We can use the emissivity profiles from the bolometer array to match peaks in the emissivity to a local temperature. From this and information about the temperatures at which peaks in radiation associated with the different species occur we can try to identify which species is responsible for the radiation peak.

Figure (4-14) shows a spatial emissivity profile (the solid line indicates the separtrix and the dashed line shows the limit of the core Thomson scattering diagnostic), while figure (4-15) shows the same emissivity profile plotted against temperature as obtained from Thomson scattering (the temperature profile is shown in Figure (4-16)).

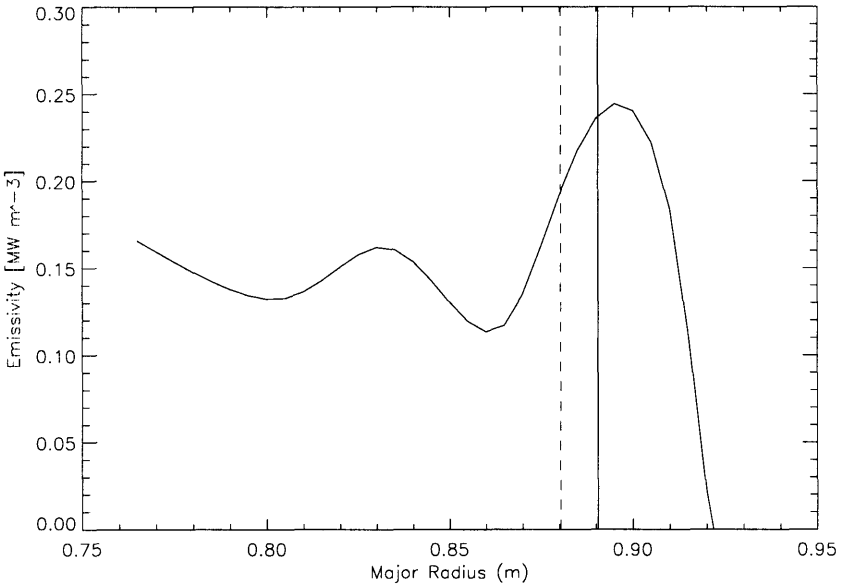

Figure 4-14: Spatial Emissivity Profile

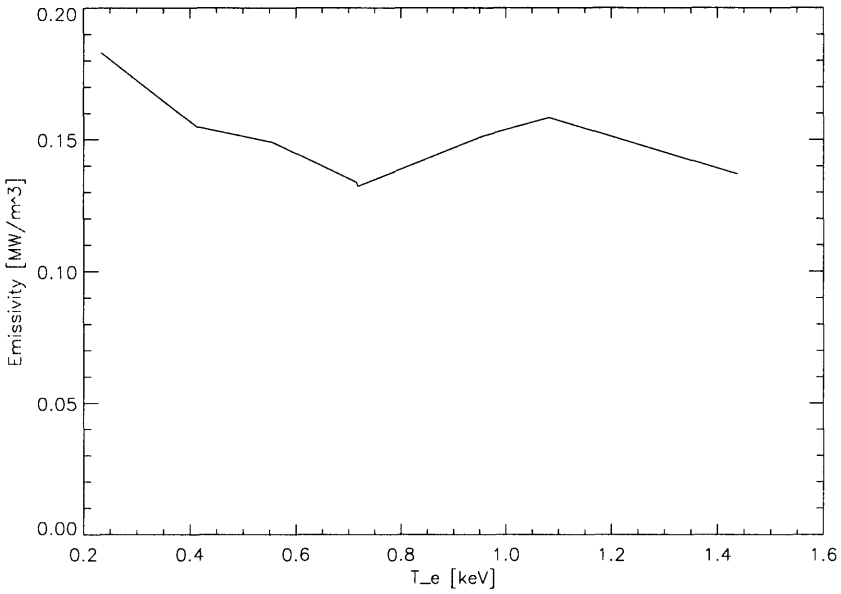

Figure 4-15: Emissivity vs. Temperature

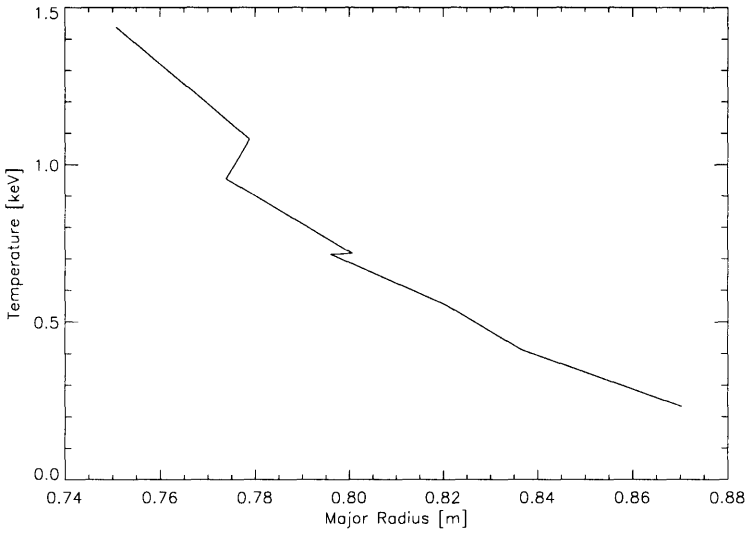

Figure 4-16: Temperature Profile

Unfortunately, this method has not been successful for the identification of the principal radiating species. Though clear peaks in the emissivity profile are observable it is not possible to reliably relate them to emission peaks of particular species. Part of the problem is that it is difficult to distinguish effects of species identity from effects of density and temperature. Recall from the Introduction, that plasma radiation is proportional to both the density and the temperature. The main difficulty, however, is that emissivity peaks as measured by the bolometer array do not reproducibly correspond to particular temperatures. As we have already seen in cases with high concentrations of injected impurities(Section 4.4) emissivity profiles corresponding to different impurity species are distinguishable. The possibility of identification does not seem to extend to typical plasmas at this time.

In this chapter several studies of the emission properties of tokamak plasmas from Alcator C-mod tokamak both in spacial profile and in total have been reported. Many of the investigations discussed here yielded negative results. As examples, it would have been useful to be able to identify impurity species present in the plasma or observe the diminution of boronization effects on the basis of the emissivity profile obtained from the bolometers. On the the other hand, we now know that studies of these properties of the plasma will not work with the current bolometer setup.

Chapter 5

Summary, Conclusions, and Future Work

5.1 Summary

This thesis is an attempt to gather together the information available about the bolometer diagnostics of the Alcator C-mod tokamak and to present some results obtained using these diagnostics. The chapters comprising the thesis deal with the fundamentals of bolometer operation and why they are useful diagnostics to have on a tokamak (including some rudimentary information about tokamaks in general and C-mod in particular), the details of bolometer operation, the use of tomographic techniques and multiple bolometric sensors to generate emissivity profiles of measured plasmas, and, finally, some results obtained using the equipment and methods discussed in the earlier sections.

5.1.1 Bolometer Basics

A bolometric diagnostic is used to measure radiated power. This diagnostic is important in a tokamak because radiation is one of the main ways the confined plasma loses energy and since energy (and particle) confinement is what we are about it is important to try to understand radiative losses as well as possible. We would like

to understand how both total radiated power and plasma emissivity profile shapes behave under a variety of plasma conditions.

5.1.2 Alcator Bolometer Details

The bolometer diagnostics of Alcator C-mod covered by this thesis are of two varieties. There are two sets of tangentially viewing bolometer arrays (for forming emissivity profiles as well as reconstructing total radiated power) one is made up of silicon photodiode detectors and the other has bridge circuits made of matched meander resistors in thermal contact with gold foils either shielded from or exposed to the radiation of interest (see Chapter 2). Similarly there are two wide aperture or 2π bolometers, one of each type as described above. Chapter two includes figures illustrating where exactly in the tokamak the detectors view as well as details of how they work.

5.1.3 Profile Reconstruction: Abel Inversion

Chapter three details the process of obtaining radial profiles of plasma emissivity from the tangentially viewing bolometer arrays via tomographic (Abel) inversion. The important equation governing this procedure is

$$e(r) = -\frac{1}{\pi}\int_r^{r_0} \frac{db}{dy}(y^2 - r'^2)^{-\frac{1}{2}} y dy \tag{5.1}$$

where $e(r)$ is the emissivity profile and $b(y)$ is the power absorbed (per unit area) by the detector with tangency radius y (see Chapter 3 for the relevant figures).

Another important topic covered in the third chapter of the thesis is the nature of error propagation through the Abel inversion. A result of [8] shows that uncertainties in the incident powers measured by the detectors produce greater errors in the emissivity profile when they come from detectors viewing closer to the center of the plasma. Another way of putting this is to say that uncertainty in the radial emissivity profile decreases as one moves out in radius. Correctly handling the errors in the profile is vitally important for making meainingful comparisons between profiles from different plasmas as discussed in the next section.

5.1.4 Results

In this section I will recaptitulate the problems whose investigation is described in chapter four, the outcome of these studies will be saved for the conclusions section. Two kinds of measurements are possible using the bolometer diagnostics of C-mod: we can measure a large fraction of the total radiated power and we can get radial emissivity profiles as discussed above. The first of these two kinds of measurements is available both from the 2π foil and by reconstruction from the tangential foil array while the second comes only from the foil array. The diode measurments are not used because of unavailablity of reliable calibrations for the photodiode detectors.

Problems of Radiated Power

The first problem to be investigated is the power radiated from plasmas where one-hundred pecent of the input power is expected to be radiated back. We would like to know how much of the radiated power is observed by the detectors and use the information to check calibrations. Another question that was studied was the way that radiated power depends on total input power and input RF power both in H mode and L mode.

Problems of Profile Shape

There are several questions that fall under the category of profile shape problems. The first problem is to determine what will serve as a "standard" emissivity profile shape so that comparisons to other profiles are easier and more informative. The next problem tackled was an attempt to connect the features of the emissivity profile to the presence of particular impurity species. One method that was tried was to use the temperature profile and information about which impurities radiate the most at which temperatures to try to identify the impurities present. Another approach that was tried was to look for unique features in the emissivity profiles of plasmas with known highly radiative impurities to see if they could be distinguished from each other and the profiles of plasmas lacking impurities. In the spirit of comparing

emmissivity profiles we move on to comparing profiles from shots with rf power input at on-axis and both inboard and outboard off-axis resonance points. Once information was obtained about shots with off-axis heating it was possible to study shots with internal transport barriers.

5.2 Conclusions

The bolometer diagnostics of Alcator C-mod provide accurate and consistent measurements of the power radiated by the tokamak plasma. At large impurity concentrations the plasma is observed to radiate essentially all of the input power. The power emitted by the plasma is dependent on both the confinement mode and the amount of power input. In both H-mode and L-mode the radiated power, as measured by both the 2π and array foil bolometers, is linearly dependent on the input power. The difference is that in the H-mode case the proportionality factor is much larger.

Profile studies proved more difficult as there was significant variability of profiles between and during shots, even when plasma conditions were matched as well as possible. Despite the difficulties and errors larger than one would like it is possible to identify the features characteristic of "typical" plasma profiles and in many cases it is also possible to identify the differences produced by changes in plasma properties or composition. Changes were observed upon the addition of argon and neon. No significant differences were observed between plasma profiles of plasmas with and without the injection of helium and lithium. A small shift in the location of peak plasma radiation was observed between shots with off-axis as opposed to on-axis RF heating. However when the RF resonance position mapped to the same plasma flux surface no differences were observable between high- and low- field side off-axis heating. Profiles for plasmas with an ITB differed from the averaged reference set of profiles only in the far edge of the plasma.

5.3 Future Work

The first improvement to be made is to extend the measurements of the foil bolometer array to the center of the plasma. The inclusion of the plasma core will make it possible to use all of the temperature and density profile data already available in conjunction with radiation profile measurements. The addition of core views should also improve the accuracy of radiated power measurements made using the foil array. The photodiode detector based diagnostics can be improved by finding a method of calibrating them reliably, the main requirement for this would be a properly calibrated source.

Further possiblities for work on continuum radiation measurements for the C-mod tokamak not limited to the existing diagnostics can be divided into a few categories. Improvements can be made to the spatial properties of the measurement and the time resolution of the detectors..

Other Views

The addition of other viewing directions oriented poloidally and at an angle to the existing bolometer array views will make it possible to obtain poloidal cross-sections of the plasma rather than just profiles. This kind of work was in fact already done at on C-mod. Cross-sections were obtained for the plasma at the entrance to the divertor using an additonal array placed at the divertor nose. These cross-sections necessarily covered only a small region of the plasma determined by their placement. Placing a bolometer array at, for example, a vertical port and aiming it poloidally and perpendicularly to the foil array would provide the kind of cross-section I am talking about. Size limitations recommend the used of a diode array so this returns to a problem of properly calibrating such a bolometer detector. Using diode detectors for this purpose will also result in the possibility of improved spatial resolution (more channels can be packed in)and improved time resolution (because, as mentioned before, photodiode detectors have faster response times).

Bibliography

[1] Hutchinson et al. First results with alcator c-mod. *Physics of Plasmas*, 1(15), 1994.

[2] I.H. Hutchinson. Course notes: Fusion energy, 2002.

[3] John Wesson. *Tokamaks.* Oxford University Press, 2004.

[4] D.E. Post and R.V. Jensen. *At. Data Nuclear Data Tables*, 20:434, 1977.

[5] Goetz et al. High confinement dissipative divertor operation on alcator c-mod. *Physics of Plasmas*, 6(5):1899–1906, 1999.

[6] G. Mast et al. A low noise highly integrated bolometer array for absolute measurement of vuv and soft x radiation. *Review of Scientific Instruments*, 62(3):744–750, 1991.

[7] Boivin et al. High resolution bolometry on the alcator c-mod tokamak. *Review of Scientific Instruments*, 70(1):260–264, 1999.

[8] T. Mei P. Neuzil. Evaluation of thermal parameters of bolometer devices. *Applied Physics Letters*, 80(10):1838–1840, 2002.

[9] I.H. Hutchinson. *Principles of Plasma Diagnostics 2nd Ed.* Cambridge University Press, 2002.

[10] Kjell Bockasten. Transformation of observed radiances into radial distribution off the emission of a plasma. *J. of the Optical Society of America*, 51(9):943–947, 1961.

[11] I.H. Hutchinson. Private communication, 2003.

[12] Jong-Sen Lee. Speckle suppression and analysis for synthetic aperture radar. *Optical Engineering*, 25(5):636–643, 1986.

[13] A.T. Ramsey and M. Diesso. Abel inversions: Error propagation and inversion reliablity. *Review of Scientific Instruments*, 70(1):380–383, 1999.

[14] D.J. Sigmar P. Helander. *Collisional Transport in Magnetized Plasmas.* Cambridge University Press, 2002.

[15] S.P. Hirshmann and D.J. Sigmar. Neoclassical transport of impurities in tokamak plasmas. 1981.

[16] W. Beil et al. Progress in impurity transport studies on textor using new vuv spectrometers with high time resolution. *ECA*, 25A, 2001.

[17] R.A. Cairns. *Radiofrequency Heating of Plasmas.* Adam Hilger, 1991.

[18] V.A. Piotrowicz and P.G. Carolan.